Application of U-Pb Geochronology Methods to the Absolute Age Determination of Secondary Calcite

NWMO TR-2013-21 December 2013

Donald W. Davis
Department of Earth Sciences
University of Toronto

nwmo
NUCLEAR WASTE MANAGEMENT ORGANIZATION
SOCIÉTÉ DE GESTION DES DÉCHETS NUCLÉAIRES

Nuclear Waste Management Organization
22 St. Clair Avenue East, 6th Floor
Toronto, Ontario
M4T 2S3
Canada

Tel: 416-934-9814
Web: www.nwmo.ca

Application of U-Pb Geochronology Methods to the Absolute Age Determination of Secondary Calcite

NWMO TR-2013-21

December 2013

Donald W. Davis
Department of Earth Sciences
University of Toronto

Document History

Title:	**Application of U-Pb Geochronology Methods to the Absolute Age Determination of Secondary Calcite**		
Report Number:	NWMO TR-2013-21		
Revision:	R000	Date:	December 2013
Department of Earth Sciences, University of Toronto			
Authored by:	Donald W. Davis		
Verified by:	Mike Hamilton		
Approved by:	Sandra Kamo		
Nuclear Waste Management Organization			
Reviewed by:	Andrew Parmenter		
Accepted by:	Mark Jensen		

ABSTRACT

Title: **Application of U-Pb Geochronology Methods to the Absolute Age Determination of Secondary Calcite**
Report No.: **NWMO TR-2013-21**
Author(s): Donald W. Davis
Company: Department of Earth Sciences, University of Toronto
Date: December 2013

Abstract
U-Pb isotopic analyses have been carried out on vein and vug secondary calcite collected at surface from Devonian carbonate rock and from drill core of Devonian and Ordovician carbonate rocks in the area of the Bruce nuclear site in southern Ontario. Analyses were carried out by laser ablation inductively coupled plasma mass spectrometry (LA-ICPMS) and by isotope dilution thermal ionization mass spectrometry (ID-TIMS). The objective of this study was to determine if an effective methodology for precision age determinations of secondary calcite mineralization could be developed based on existing geochronological techniques. This report describes the methods employed and initial results.

Previous studies have revealed a number of differently oriented fracture sets within the Devonian carbonate rocks of the Lucas Formation exposed at surface. LA-ICPMS dating shows that veins of different orientation share the same pattern of ages. This pattern is characterized by a broad peak of ages around 110 Ma with a minor peak around 56 Ma. ID-TIMS data from surface samples appear to confirm the pattern of two ages shown by the LA-ICPMS data and suggest that calcite growth took place over a protracted period from at least 110-85 Ma with reactivation at approximately 50 Ma. The comparability of ages yielded using the two methods supports the reliability of the results.

Data on calcite in veins collected from drill core samples of the Devonian Lucas Formation at a vertical drill length of 34 m below ground surface indicate a similar age pattern to surface veins. These near-surface calcite veins contain U concentrations generally in the range of 1-10 ppm with moderately to highly radiogenic Pb. Conversely, calcite-filled veins in drill core samples from the deeper Ordovician formations are generally thinner (hairline- to mm-scale apertures) than surface and near-surface veins and the analysed material shows order of magnitude lower U concentrations and less radiogenic Pb. Only a small number of deep Ordovician samples, including one from the Collingwood Member of the Trenton Group and one from the Coboconk Formation of the Black River Group, met the criteria in terms of isotope concentrations needed to provide meaningful ages. Age determinations from these samples are less precise but the data suggest a much older age for fracture formation and vein emplacement (445 ± 42 Ma) that approaches the Paleozoic depositional age of the host rock.

The data suggest that the calcite veins in the deep Ordovician Trenton and Black River groups were formed in the Paleozoic era shortly after deposition of the host rock and contemporaneous with the Taconic Orogeny. Fracturing and emplacement of the calcite veins within the Devonian Lucas Formation appears to have occurred during the middle Cretaceous with additional calcite crystal growth during the early Paleogene. No evidence is seen for more recent (e.g., Pleistocene) vein calcite growth in either the shallow Devonian or deep Ordovician formations.

TABLE OF CONTENTS

LIST OF TABLES

Page

LIST OF FIGURES

Page

1. INTRODUCTION

This report describes the methods and initial results from application of uranium-lead (U-Pb) geochronology techniques, including laser ablation inductively-coupled mass spectrometry (LA-ICPMS) and thermal ionization mass spectrometry (ID-TIMS), to the absolute age determination of secondary vein and vug calcite from Paleozoic sedimentary rocks of the Michigan Basin in southern Ontario, Canada (Figure 1). The objective of this study was to determine if an effective methodology for precision age determinations of secondary calcite mineralization could be developed based on existing geochronological techniques. Success of this study would be reflected in the coincidence, or lack thereof, of absolute ages yielded by the two different techniques applied to sample material from the same vein or vug feature. If successful, the absolute timing of secondary calcite emplacement could be understood in terms of the Phanerozoic evolution of the Michigan Basin.

U-Pb isotopic data on vein and vug calcite and its carbonate host rock is reported herein for eight samples. This includes 4 samples (1 Devonian, 3 Ordovician) from core retrieved from boreholes drilled at the Bruce nuclear site and 4 samples collected from bedrock of Devonian age exposed along the Lake Huron shoreline (Figure 1, Table 1). The secondary calcite in the Ordovician samples occurs as hairline to mm-scale veins and mm-scale vugs (e.g., Figure 2). The secondary calcite in the Devonian samples occurs in distinctly-oriented families of mm-scale veins where observed in surface exposed bedrock (e.g., Figure 3), and as irregularly oriented vein and vug systems in drill core. An additional eight Ordovician samples were originally selected to be included in this study. However, preliminary spot LA-ICP-MS analyses on individual calcite grains within calcite veins hosted by these samples measured almost no detectable U or Th (Thorium), and generally very low Pb concentrations precluding their usefulness as geochronometers. These additional samples are not reported on herein.

Geochronological analysis of the Devonian samples provides a means of testing a recent hypothesis for the timing of vein emplacement that was based on detailed local field observations and regional fracture patterns. Cruden (2011) used geometrical arguments and cross-cutting relationships to suggest that the fracture network observed in the Devonian bedrock proximal to the Bruce nuclear site, including secondary calcite veins, was emplaced during a middle Devonian period of extension related to tectonic subsidence of the Michigan basin (e.g., Howell and van der Pluijm 1999). Therefore, any reliable absolute age information for secondary calcite from within the Devonian samples examined during this study would be used to re-assess this initial hypothesis.

The purpose of collecting and studying secondary calcite hosted in the Ordovician samples is to better understand the evolution of the secondary fracture network in these deeply (> 400 m) buried sedimentary rocks. The Ordovician sedimentary rocks represent the host (Cobourg Formation) and primary barrier sequences (overlying Upper Ordovician shales and underlying Upper Ordovician carbonates) for a proposed Deep Geological Repository (DGR) for Low and Intermediate Level Waste (L&ILW) from Ontario Power Generation's (OPG) owned or operated nuclear generating facilities (NWMO, 2011). The calcite-filled veins and vugs within the collected samples provide evidence that fluid migration events have occurred in these rocks at some point in the geologic past. This secondary fracture network also represents a potential future pathway. The determination of absolute timing constraints for this secondary fracture network can therefore provide insight into the future containment and isolation capabilities of the proposed host rock. The opportunity would also be present to compare and contrast the temporal relationship between the deep and shallow fracture networks. The results will aid in our understanding of the long-term stability of deep seated groundwater regimes within the Paleozoic age sedimentary rocks of southern Ontario. In addition, this research will support future site investigations in both sedimentary and crystalline rock environments.

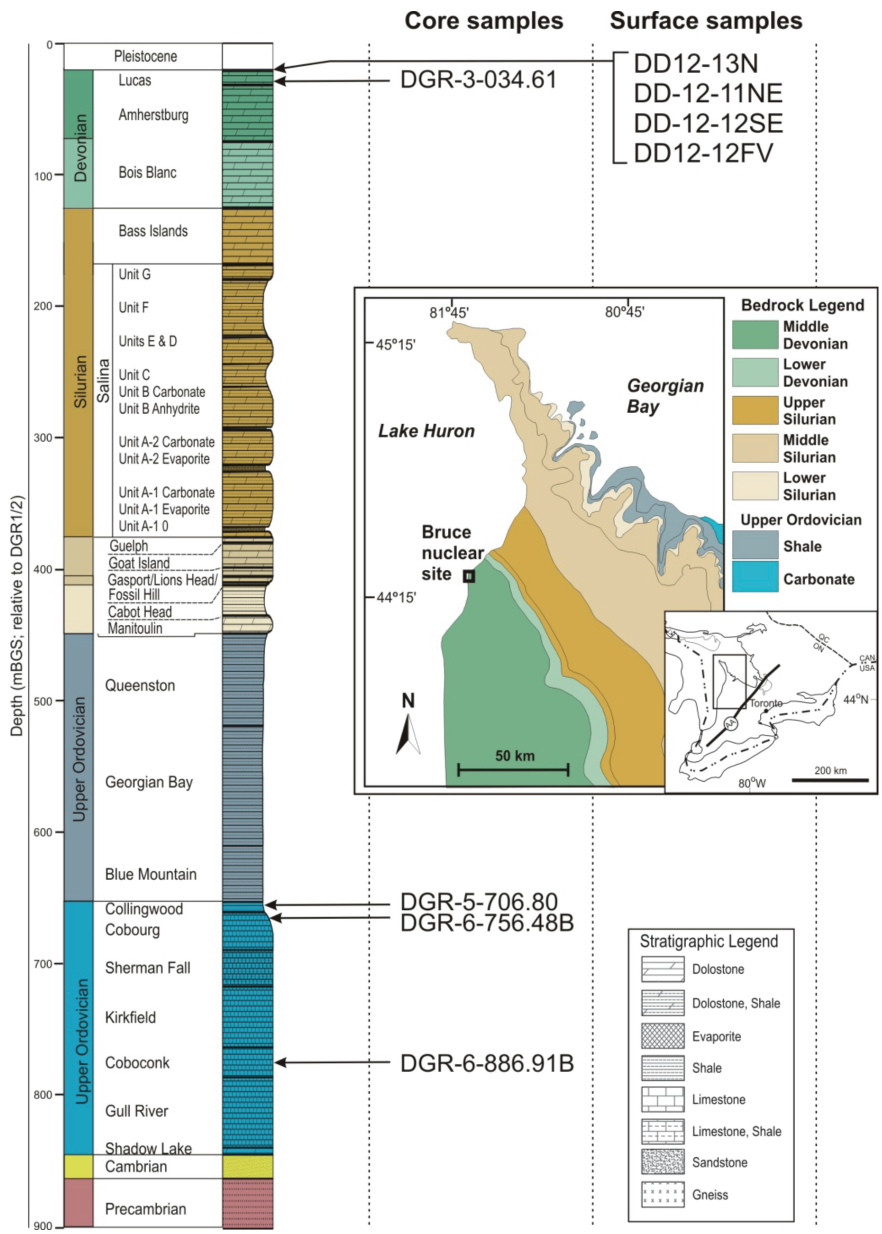

Figure 1: Representative Paleozoic Stratigraphic Column for the Bruce Nuclear Site Showing the Approximate Stratigraphic Location of Numbered Core and Surface Samples Used in this Study. Stratigraphy is Based on Core Logging of Boreholes DGR-1/2 (Intera, 2011). Depth is in metres Below Ground Surface (mBGS). Inset Maps Show Bedrock Geology Surrounding the Study Location and the Surface Trace of the Algonquin Arch (AA) Across Southern Ontario

Chapter 2 provides a description of the geological setting of the Paleozoic sedimentary sequence encountered at and beneath the Bruce nuclear site (Figure 1), including a brief overview of the tectonic history of the southern Ontario portion of the Michigan Basin. Chapter 3 describes the LA-ICPMS and ID-TIMS methods applied to the samples. Chapter 4 describes the results from the LA-ICPMS and ID-TIMS analyses. Chapter 5 includes a discussion of the results. Conclusions are presented in Chapter 6, followed by Acknowledgements and References.

Table 1: Sample List for LA-ICPMS and ID-TIMS Analyses

Sample #	Formation (Fm) or Member	Surface or Core sample	Morphology	Methods Used (LA-ICPMS/TIMS)
DD-12-11NE	Devonian Lucas Fm	Surface	NE-trending mm-scale sub-vertical vein	LA-ICPMS/TIMS
DD12-12SE	Devonian Lucas Fm	Surface	SE-trending, mm-scale sub-vertical vein	LA-ICPMS
DD12-12FV	Devonian Lucas Fm	Surface	Sub-horizontal mm-scale vein	LA-ICPMS/TIMS
DD12-13N	Devonian Lucas Fm	Surface	N-trending mm-scale sub-vertical vein	LA-ICPMS
DGR-3-034.61	Devonian Lucas Fm	Core	Unoriented mm-scale vein array	LA-ICPMS/TIMS
DGR-5-706.80	Ordovician Collingwood Member	Core	Unoriented mm-scale vein	TIMS
DGR-6-756.48B	Ordovician Cobourg Fm	Core	Unoriented mm-scale vein-vug system	TIMS
DGR-6-886.91B	Ordovician Coboconk Fm	Core	Unoriented hairline vein	LA-ICPMS/TIMS

2. GEOLOGICAL SETTING

Southern Ontario is underlain by Upper Cambrian to Devonian/Mississippian sedimentary rocks resting unconformably upon Precambrian basement of the Grenville Province of the Canadian Shield. The oldest Paleozoic rocks of southern Ontario include a thin veneer of Late Cambrian clastic-dominated sediments unconformably overlying the Precambrian basement. These rocks, deposited during the initial development of the Michigan Basin, pinch out further to the east along the flank of the Algonquin Arch (Figure 1; e.g., Bailey and Cochrane 1984a, Bailey and Cochrane 1984b). The Cambrian units are unconformably overlain by Ordovician-aged sediments. The Ordovician stratigraphy dips gently to the southwest towards the centre of the Michigan Basin. Deposition occurred over a broad carbonate and clastic shelf and platform setting that extended from the eastern margin of the Appalachian Basin to the centre of the continent. Deposition during the Silurian, within the subsiding Michigan Basin, produced more complicated basin-centred assemblages which include for example, reef and evaporite facies.

Onset of Devonian deposition is represented by a major marine transgression after a long period of exposure at the end of the Silurian (Uyeno et al. 1982).

The Paleozoic stratigraphy at the location of the Bruce nuclear site is shown in Figure 1. Drilling and core logging of boreholes DGR-1 to DGR-6 at the Bruce nuclear site led to the identification of 34 distinct Paleozoic bedrock formations, members, or units of approximately 840 metres cumulative thickness beneath a thin veneer (7 to 20 m) of Pleistocene overburden and unconformably overlying Precambrian granitic gneiss (Intera 2011). The reference Paleozoic sequence, based on core logging of the DGR-1 and DGR-2 boreholes, comprises 104.0 m of Devonian dolostone, 323.7 m of Silurian dolostone, argillaceous dolostone, shale and evaporite, 211.8 m of Upper Ordovician shale, 179.1 m of Upper Ordovician argillaceous limestone, 5.2 m of Ordovician siltstone and sandstone, and 16.9 m of Cambrian sandstone.

The Paleozoic succession was deposited northwestward of the Appalachian Orogen, a mountain chain that formed during the protracted closure of the Iapetus Ocean and assembly of the Pangaean Supercontinent (e.g., Williams and Hatcher 1982). Southern Ontario is underlain by two main paleo-depositional centres referred to as the Appalachian and Michigan basins. The former is a foreland basin to the Appalachian orogen while the latter is a broadly circular intracratonic basin. In southern Ontario, these basins are separated by the northeast-trending Algonquin Arch which defines a regional basement high (Figure 1 inset map). The Algonquin Arch is one of several named basement arches that acted as structural and topographic controls on depositional patterns during the Paleozoic Era (e.g., Sanford et al. 1985), rising and falling with respect to the Michigan and Appalachian Basins in response to vertical epeirogenic movements, horizontal tectonic forces, and subduction at the orogenic front (Quinlan and Beaumont 1984, Coakley and Gurnis 1995, Leighton 1996, Howell and van der Pluijm 1999, Nadon et al. 2000).

Three main pulses of tectonic activity are contemporaneous with variations in regional depositional patterns within the Michigan Basin. These include the Taconic (Ordovician), Caledonian/Acadian (Silurian-Devonian) and Alleghenian (Carboniferous-Permian) events (Sanford et al. 1985). The Taconic Orogeny is characterized by large-scale eastward-tilting of the Laurentian margin and departure of the depositional geometry of the Michigan Basin from its concentric, basin-centered pattern (Coakley et al. 1994, Coakley and Gurnis 1995, Howell and van der Pluijm 1999). This allowed for deposition of the laterally extensive Ordovician limestone and overlying shale successions. A regionally recognized bentonite layer dated at ca. 454 Ma is interpreted as ash fall preserved from major (calc-alkaline) volcanic activity that occurred along the southeastern Laurentian margin during Taconic orogenesis (Huff et al. 1992, Kolata et al. 1998).

The Late Silurian Caledonian phase of the Acadian Orogeny, driven by the collision between the North American and African plates, rejuvenated the Algonquin-Findlay arch system and returned the Michigan Basin to its concentric geometry (e.g., Quinlan and Beaumont 1984, Howell and van der Pluijm 1990). Upper Silurian evaporites of the Salina Group were deposited at this time under restricted marine conditions (Johnson et al. 1992, Armstrong and Carter 2010). A major unconformity reflects emergent conditions at the end of the Silurian. Foreland loading during the middle to late Devonian characterizes the main pulse of the Acadian event. Tectonism was concomitant with renewed platform margin subsidence that allowed another marine incursion into the Michigan Basin across the subdued arch system (Quinlan and Beaumont 1984, Armstrong and Carter 2010). Early Mississippian uplift of the arch system once again starved the Michigan Basin as it regained its concentric form (Quinlan and Beaumont 1984). The Alleghenian Orogeny was the last active tectonic event to stimulate significant sediment deposition in the Appalachian foreland during the Carboniferous, Permian, and likely early Mesozoic times. Peak sediment burial in the Michigan Basin is thought to have occurred during this timeframe (e.g., Coniglio and Williams-Jones 1992; Wang et al. 1994).

Active orogenesis throughout eastern North America, a common characteristic of much of the Paleozoic Era, transitioned to a passive margin extensional setting when the Atlantic Ocean began to open at the end of the Triassic Period approximately 200 Ma. Much of the resulting tectonic activity was concentrated near the continental margin, where Triassic and Lower Jurassic rift basin deposits record the onset of continent break-up (e.g., Lindholm 1978). Further inland, the majority of rift-related deformation and sediment deposition occurred in proximity to the trace of the Appalachian thrust front (Wheeler 1995). Pre-existing faults, including those of the Neoproterozoic to Early Cambrian (Iapetan) St. Lawrence rift system and the Ottawa-Bonnechere Graben structure, were re-activated as a system of NE-striking extensional normal faults and WNW-striking transfer faults (Thomas 2006). These areas of re-activation remain seismically active to the present day (Kumarapeli and Saull 1966, Adams and Basham 1991).

Mesozoic magmatic activity in eastern North America is marked by kimberlites and other mafic intrusions within the Canadian Shield (Heaman and Kjarsgaard 2000), and the alkaline intrusion of the ca. 130-110 Ma Monteregian Hills and White Mountain magma series, which are the most prominent features of the New England-Quebec igneous province (McHone and Butler 1984), and the offshore basaltic New England Seamounts (McHone 1996). These magmatic events may record the Jurassic to Cretaceous northwesterly movement of North America as it passed above the Great Meteor hotspot (e.g., Crough 1981, Legall et al. 1981, Morgan 1983, Heaman and Kjarsgaard 2000). Other magmatic activity includes Middle Jurassic ultramafic dykes dated at 173 Ma (K-Ar method; Barnett et al. 1984) which intrude Middle Ordovician strata in the Picton Quarry, Ontario. Dyke emplacement is believed to be related to fault reactivation and the dykes are also interpreted to have been offset by E-trending brittle strike-slip faults (McFall 1990). Late Jurassic ultramafic dykes in the Finger Lakes region of New York State are spatially coincident with the Clarendon-Linden fault system located to the south of Lake Ontario (Heaman and Kjarsgaard 2000). The majority of recognized Mesozoic magmatic activity is localized around pre-existing faults which are a considerable distance away from the study area at the Bruce nuclear site.

A Late Cretaceous to Eocene global-scale plate re-organization event resulted in the transition from northwesterly to west-southwesterly North American motion (Minster and Jordan 1978, Rona and Richardson 1978, Gordon and Jurdy 1986). Contemporaneous onset of southwest-northeast spreading in the North Atlantic, coincident with impingement of the Iceland Plume, may have initiated the east-northeast-oriented compressional stress field that controls the neotectonic evolution of eastern North America (Sbar and Sykes 1973, Zoback and Zoback 1989). A regionally persistent east-northeast-trending joint set is one possible manifestation of this contemporary stress (Engelder 1982).

3. METHODS

U and Pb isotopes were analyzed in two sessions. Initial measurements in each session were taken using laser ablation inductively-coupled mass spectrometry (LA-ICPMS) in order to identify grains with relatively high U and low common Pb contents. These grains were subsequently analyzed in the second session using more precise and accurate thermal ionization mass spectrometry (ID-TIMS). LA-ICPMS sensitivity was too low to obtain reliable age information during the first session. The pumping capacity of the LA-ICPMS expansion chamber was subsequently increased by addition of a large 75 l/sec rotary pump (S-option). This enhanced sensitivity for Pb and U by about a factor of five and allowed reliable age information to be derived from the LA-ICPMS measurements.

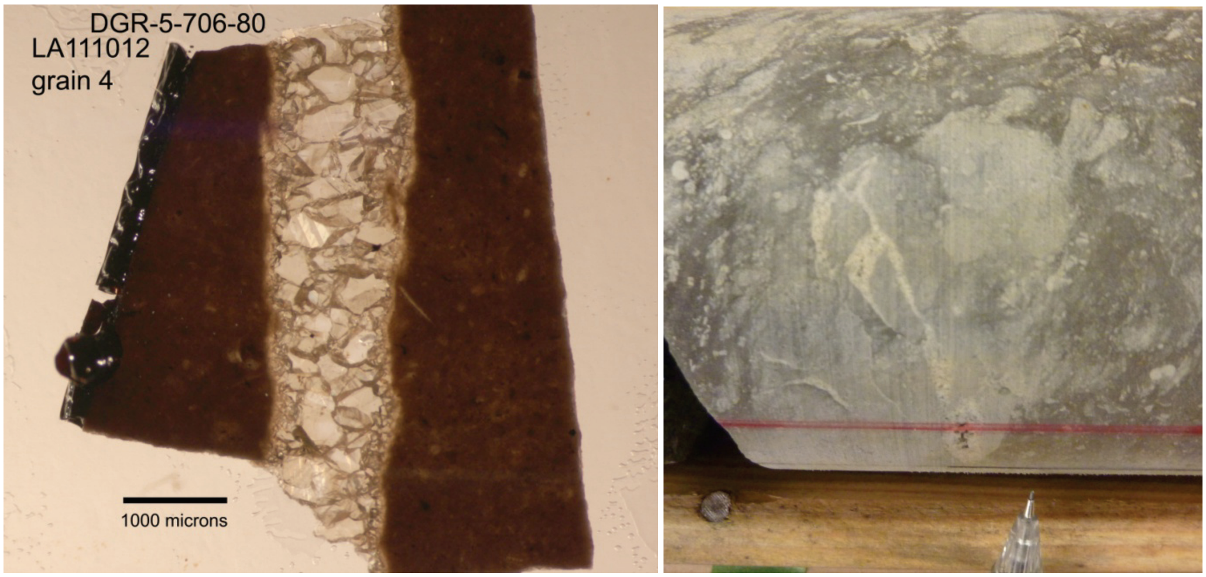

Figure 2: Left - Thin Section Sample of Calcite Vein in Drill Core from an Ordovician Sample (DGR-5-706.90). Right - Vein-vug System in Ordovician Drill Core Sample (DGR-6-756.48B; pencil tip for scale)

Figure 3: Three Intersecting Families of Calcite-filled Veins in Exposed Devonian Bedrock Along the Lake Huron Shoreline Near the Bruce Nuclear Site

Calcite from veins in core samples was taken from thin sections. Calcite crystals from surface veins were removed by sawing out as much of the host carbonate as possible and removing the rest by careful abrasion with sandpaper. Crystals with little or no attached visible brownish carbonate were mounted on double-sided tape and the ground side was targeted for analyses (Figure 4 - top). Spots are generally located close to the margin of the samples in order to precisely document locations during analysis. It is difficult to locate areas in the middle of clusters because of the lack of visible markers. During a second session, single crystals or crystal clusters were mounted with the ground side against parafilm and the natural surfaces of crystals were targeted (Figure 4 - bottom).

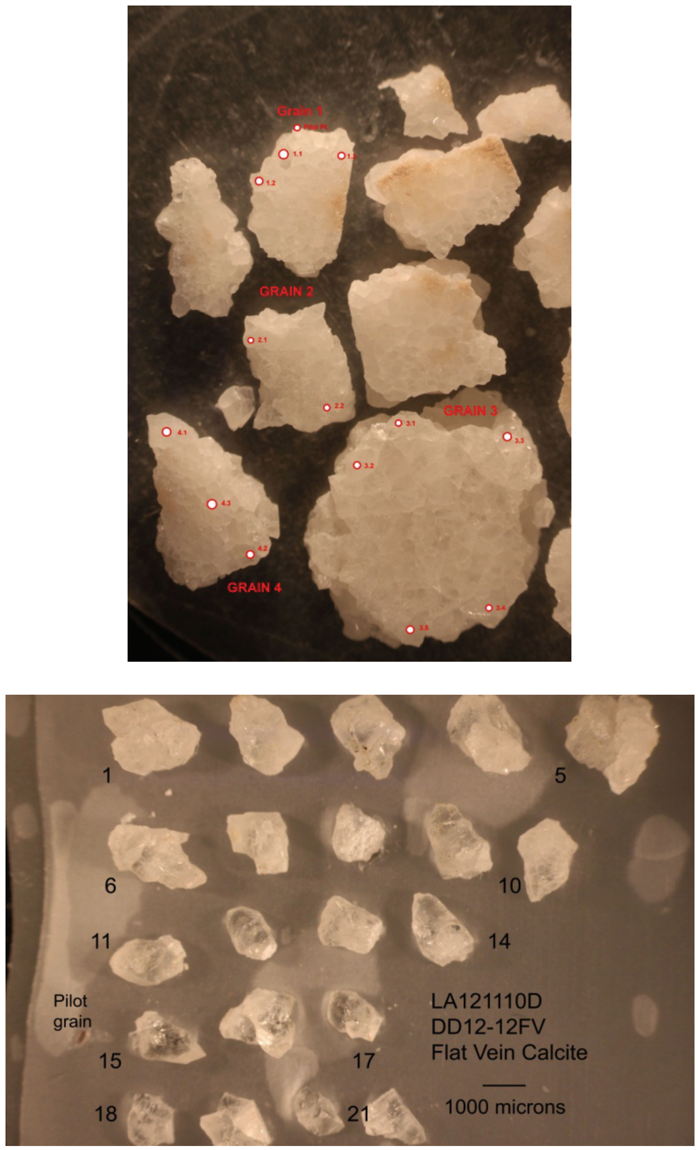

Figure 4: Top - Thin Section Devonian Calcite Crystals from Surface Samples Targeted by LA-ICPMS on Ground Basal Surfaces. Numbered Circles Indicate Laser Spot Analyses. Bottom - Calcite Targeted by LA-ICPMS on Natural Surfaces of Devonian Calcite Crystals Collected from Surface Veins

3.1 LASER ABLATION INDUCTIVELY COUPLED PLASMA MASS SPECTROMETRY (LA-ICPMS)

Samples were ablated using a 100 micron diameter UV laser beam with a wavelength of 213 nm (New Wave UP-213 laser ablation system). The ablated material is carried by He into an ionizing plasma and Pb and U isotopes analyzed using a quadrupole mass spectrometer (VG Series 2 Plasmaquad). The laser was operated at 10 Hz and 40% power. Data were collected on ^{88}Sr or ^{43}Ca (10 ms), to measure the efficiency of ablation and ^{232}Th (10 ms) to test for the presence of detrital or host rock material. Data on ^{206}Pb (40 ms), ^{207}Pb (40 ms) and ^{238}U (20 ms) furnish age information. Immediately prior to each analysis, the spot was pre-ablated by rastering the beam over an area larger than the beam diameter for about 15 sec (2-3 sweeps) to clean the surface. Following a 10 sec period of baseline accumulation the laser sampling beam was turned on and data were collected for 35 seconds followed by a 50 sec washout period. The laser beam was observed to often cleave off large pieces of the calcite target so the holes tend to be irregular (Figure 5). This is probably because about half of the calcite is transformed into CO_2 during ablation by the 213 nm beam (Münsterer et al. 2011). NIST-610 and NIST-612 glasses were used as standards.

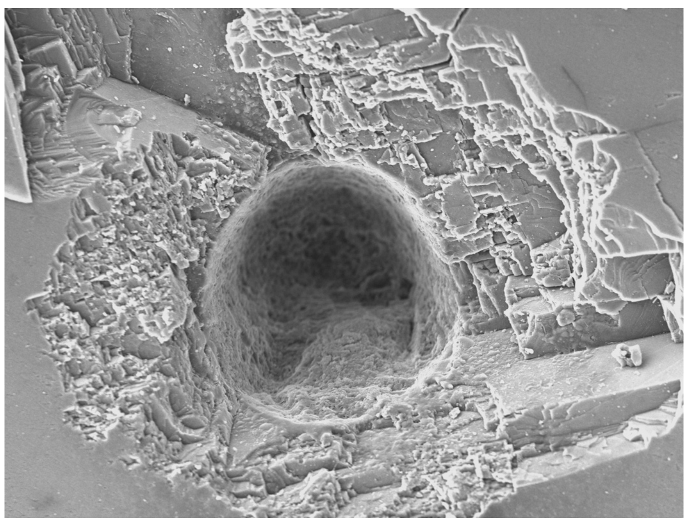

Figure 5: Polished Calcite after Laser Ablation from Analytical Session 2

3.2 ISOTOPE DILUTION THERMAL IONIZATION MASS SPECTROMETRY (ID-TIMS)

For the first analytical session, fragments of calcite from core were broken from thin section slabs (Figure 4), taking care not to include carbonate host material, and washed in MilliQ water and alcohol. Picked fragments were transferred into a clean 3 ml Savillex vial under clean air conditions by electrostatic adhesion to a small strip of Parafilm. Calcite was dissolved in purified 3N HCl, ^{205}Pb-$^{233,235}U$ spike was added (ET535 EarthTime spike) and the sample was dried. The sample was redissolved in 10 drops of 3N HCl and loaded onto 50 microlitre anion exchange columns. U was eluted and Pb washed in 1N HBr. Pb was eluted with 6N HCl into a Savillex vial and dried. The U solution was dried down and U redissolved in 6N HCl and reloaded onto the column, U was washed with 6N HCl and 7N HNO_3, then eluted with H_2O into a separate Savillex vial and dried. Pb was dissolved again in HBr and loaded onto a new clean anion exchange microcolumn, washed and eluted as before. One drop of 0.05N H_3PO_4 (phosphoric acid) was added and the eluate was dried. Phosphoric acid is hygroscopic so the sample can be easily located after dry-down. The column was converted to 6N HCl, the U fraction was redissolved in 6N HCl and loaded onto the second column, then washed as above with 6N HCl and 7N HNO_3, and eluted with H_2O into a separate Savillex vial. One drop of H_3PO_4 (phosphoric acid) was added and the eluate was dried. A first attempt at calcite analysis was processed using only one cycle of column chemistry. This resulted in very weak Pb emission. Samples processed with two column chemistry all produced strong stable emission for both Pb and U.

Relatively large crystals with well-defined LA-ICPMS ages and relatively high radiogenicity taken mostly from surface samples (Figure 4) were chosen for a second ID-TIMS analytical session. Crystals were leached for about 15 sec in 0.5 N HCl to remove surface contamination. The crystals were then transferred into a clean 3 ml Savillex vial as above and dissolved in purified 3N HCl. ^{205}Pb-$^{233,235}U$ spike was added (ET535 EarthTime spike) and the sample was dried. Two different approaches were tried to separate Pb and U with a minimum for contamination. In the first, the sample was redissolved in 3N HCl and loaded onto clean large 500 microlitre anion exchange columns. The columns were washed using about 1 ml 3N HCl. Pb was then eluted in 1 ml 6N HCl followed by U in 1 ml H_20 into the same vial. One drop of 0.05N H_3PO_4 (phosphoric acid) was added and the eluate was dried. Half of the solutions for two samples were loaded onto clean Re filaments with Si-gel for isotopic analysis on a VG354 mass spectrometer. These were found to give less robust emission than expected, so the samples were passed through the columns for a second time.

A second, simpler approach was tried on two of the samples. The dried samples were redissolved in a few drops of 3N HCl and transferred with spike to 1.5 ml polypropylene centrifuge tubes. About 1 ml of concentrated HF was added, which resulted in precipitation of most of the Ca as CaF_2. After centrifugation, most of the supernatant was drawn off and transferred to the washed dissolution capsule. Half of each solution was loaded onto Re filaments with silica gel for TIMS analysis. The first sample showed no signal whatsoever, suggesting that the sample had fallen off or silica had been removed. Examination of the second load showed crystalline material rather than glass, suggesting that the presence of residual fluoride resulted in loss of silica as gaseous SiF_4. The SiO_2 acts to both retain Pb to high temperature and as an ionization activator. It is essential for obtaining measureable beams. A drop of concentrated silica gel was added to this load and it was possible to measure its isotopic ratios, although signal strengths were about ten times less than normal. The second half of each sample solution was then passed through anion exchange 50 microliter columns and Pb and U eluted. These samples emitted normally on the mass spectrometer.

TIMS analyses were carried out using a Daly collector in pulse counting mode. Dead time and fractionation corrections are regularly monitored using the SRM982 Pb standard. After Pb analyses were completed, the U fractions were loaded onto their respective Pb filaments with Si-gel and analyzed as for Pb. The Pb fractions were loaded and analyzed first to minimize Pb blank. A blank determination carried out with the samples gave 1 picogram Pb and <0.01 picogram U.

4. RESULTS

Pb isotopic data are reported in Table 2 for LA-ICPMS and Table 3 for ID-TIMS. These data are included at the end of the report. Results are plotted on Wetherhill concordia diagrams ($^{206}Pb/^{238}U$ vs. $^{207}Pb/^{235}U$, Figures 6 to 14). Errors on diagrams and in the text are reported at two sigma. Plotting and data regressions were carried out using Isoplot software (Ludwig 2003). U decay constants are from Jaffey et al. (1971).

Because of the low proportion of ^{207}Pb in Phanerozoic radiogenic Pb and the high proportion of common Pb in the samples, $^{206}Pb/^{238}U$ is the most reliable ratio for age determination. This is the concordia intercept age of a horizontal line passing through the data. For ID-TIMS data, measured ^{206}Pb and ^{207}Pb are corrected for initial common Pb based on measurements of ^{204}Pb. For LA-ICPMS data, ^{204}Pb cannot be measured accurately so measurements of total Pb/U isotopes are plotted. The presence of significant common Pb has the effect of shifting data to the right and upward towards an age of approximately 5000 Ma (Figure 6). Hence, multiple data with a similar age but different levels of common Pb will form a linear array on the concordia plot with the lower concordia intersection giving the age of the radiogenic component. Model ages are calculated for each LA-ICPMS datum in Table 2 (see pg x) by projecting along a radiogenic-common Pb mixing line to concordia, assuming a $^{207}Pb/^{206}Pb$ ratio of 0.83 for the common Pb based on the Stacey and Kramers (1975) growth curve.

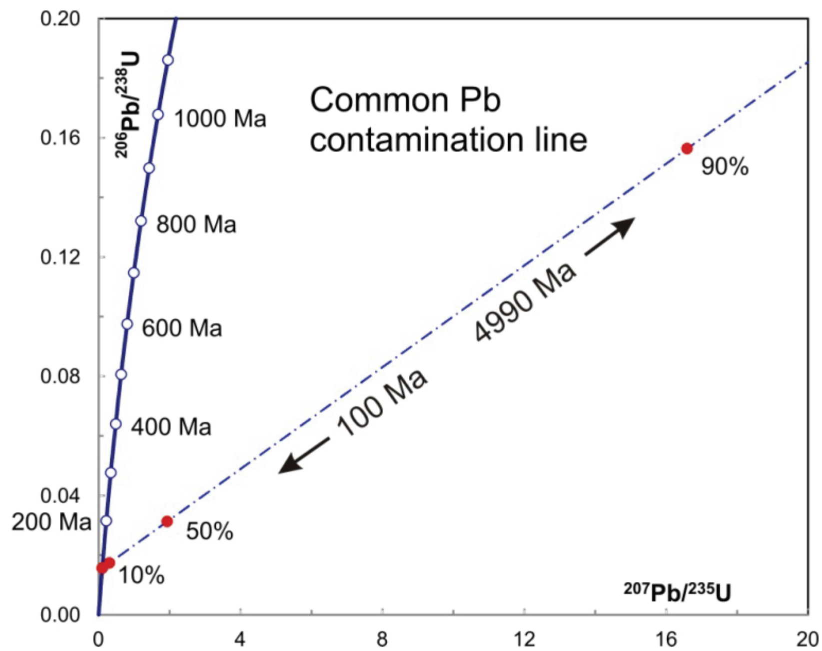

Figure 6: U-Pb Concordia Plot Showing the Effect of Adding Different Amounts of Common Pb to a 100 Ma Old Sample. Percentages Represent Proportions of Common Pb (with a $^{207}Pb/^{206}Pb$ ratio of 0.83) in the ^{206}Pb Signal

4.1 LA-ICPMS RESULTS

4.1.1 Whole Grains

The first set of LA-ICPMS measurements that gave useful age information were carried out on basal surfaces of crystal clusters from which the host carbonate had been removed by grinding (Figure 4 - top). A second set of measurements was carried out on natural crystal surfaces of grains fixed on parafilm (Figure 4 - bottom).

4.1.1.1 DD12-11NE Northeast-trending Surface Vein (Devonian Lucas Formation)

The data from analytical session 1 all show a significant common Pb component (black ellipses on Figure 7). The most contaminated datum shows evidence for an older radiogenic component and is off scale on Figure 7. The second session on natural surfaces of crystals produced data that are all near-concordant (red ellipses on Figure 7). Ground samples did not show less radiogenic compositions relative to natural surfaces for other samples and, in fact, are on average more radiogenic for sample DD12-13 (discussed below). The common Pb is most likely derived from small amounts of residual host rock that had not been completely removed from this sample. Most data are clustered around a $^{206}Pb/^{238}U$ age of about 100 Ma but a few appear slightly older or younger extending the range from about 80-140 Ma. Regressing the data with the 2 oldest and 2 youngest data omitted gives an average age of 99 ± 3 Ma (Mean Square Weighted Deviation; MSWD – 3.2).

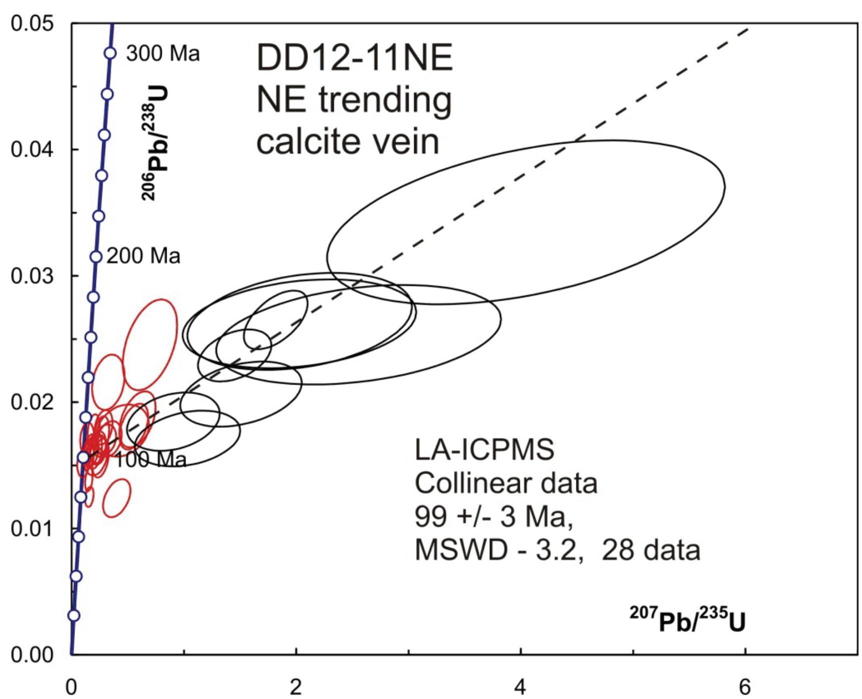

Figure 7: Concordia Diagram Showing LA-ICPMS Data (n = 28) from Northeast-trending Calcite Veins in Sample DD12-11NE. Black Ellipses are from Targeting Ground Surfaces While Red Ellipses are from Natural Crystal Surfaces. The Two Oldest and Two Youngest Data are Omitted from the Regression

4.1.1.2 DD12-12SE Southeast-trending Surface Vein (Devonian Lucas Formation)

Data show a fairly consistent common Pb contamination trend. Precise near-concordant data are again clustered around about 100 Ma but one datum is distinctly younger at about 50 Ma (black partial ellipse to the right of concordia in Figure 8) while several may be distinctly older at 120-140 Ma (Figure 8). Omitting the ca. 50 Ma datum, which is clearly an outlier that may represent a later generation, gives a regression age of 104 ± 6 Ma (MSWD – 13).

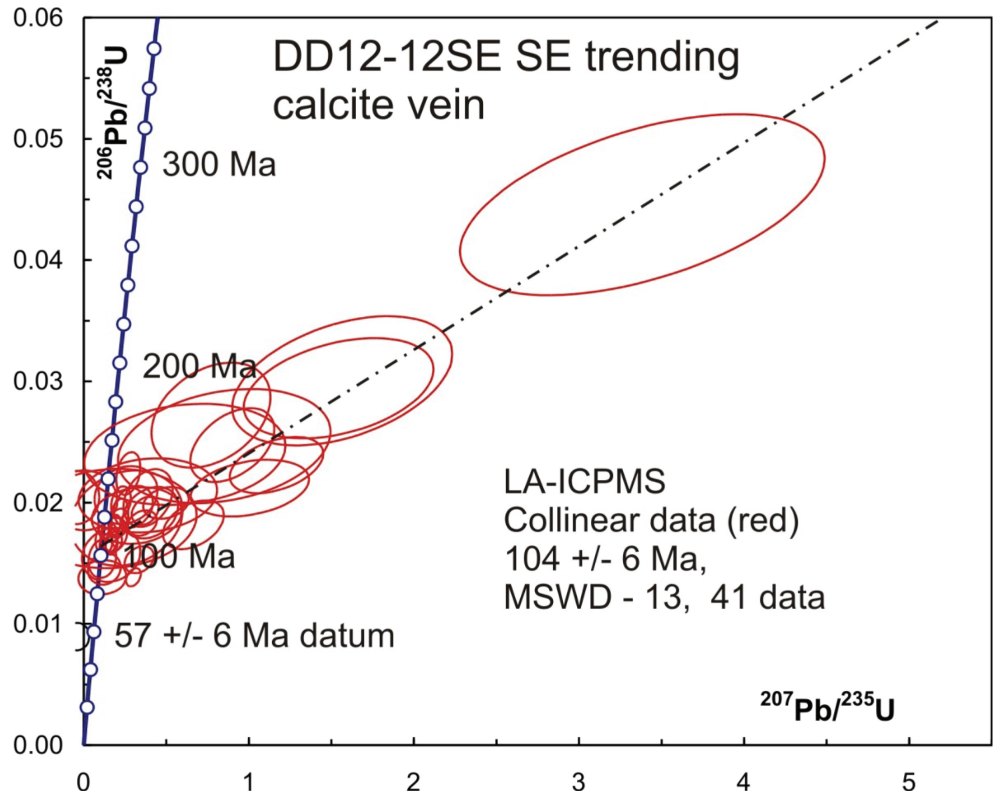

Figure 8: Concordia Diagram Showing LA-ICPMS Data (n = 41) from Southeast Trending Calcite Veins in Sample DD12-12SE. One Distinctly Younger Analysis (black partial ellipse) is Omitted from the Regression

4.1.1.3 DD12-12FV Flat Surface Vein (Devonian Lucas Formation)

This is from a horizontal vein set from the same sample that contained the SE trending set. Fewer of the analyses are near-concordant but those that are again show a distinct age spread for the most precise analyses (Figure 9). A roughly collinear subset gives an age of 102 +/- 7 Ma (MSWD – 5.5) but there are distinct near-concordant data at about 50 Ma and 120 Ma.

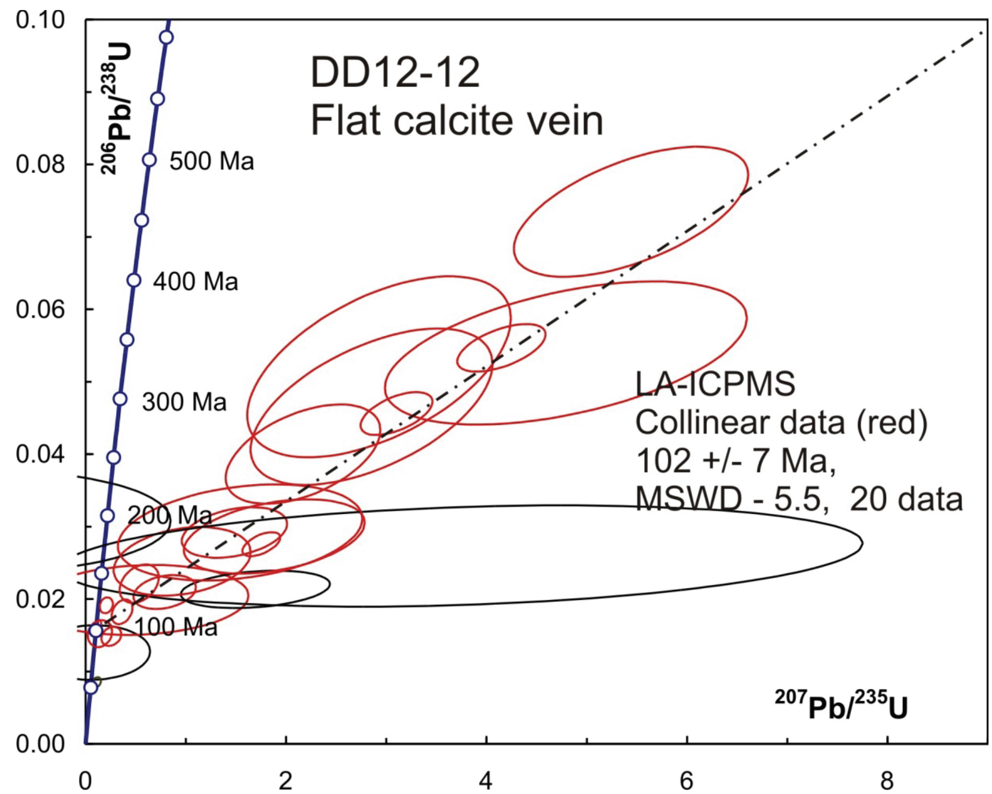

Figure 9: Concordia Diagram Showing LA-ICPMS Data (n = 20) from Flat Calcite Veins in Sample DD12-12FV. Black Ellipses are Omitted from the Regression

4.1.1.4 DD12-13N North-trending Surface Vein (Devonian Lucas Formation)

Concordia data show a relatively dispersed pattern for the high common Pb analyses but these and many near-concordant data are consistent with an age of around 100 Ma (shown in red on Figure 10). One analysis was carried out on a calcite vein in slab section and one on the adjacent limestone host rock. These ellipses are labelled and shown in black on Figure 10. They are relatively high in common Pb and also show evidence for an older radiogenic Pb component, especially the host rock analysis. Omitting the five youngest analyses (also shown in black on Figures 10 and 11), the remaining 37 data define an average model age of 99 ± 7 Ma but with excess scatter (MSWD – 7.5). Averaging only the near-concordant older data from separated calcite crystals (shown in red on Figure 11) defines an average of 104 ± 5 Ma but this cluster also shows excess scatter (MSWD – 5). Three precise analyses from three different grains (shown in black on Figure 11) overlap at a distinctly younger age of 57 ± 3 Ma (MSWD – 0.8).

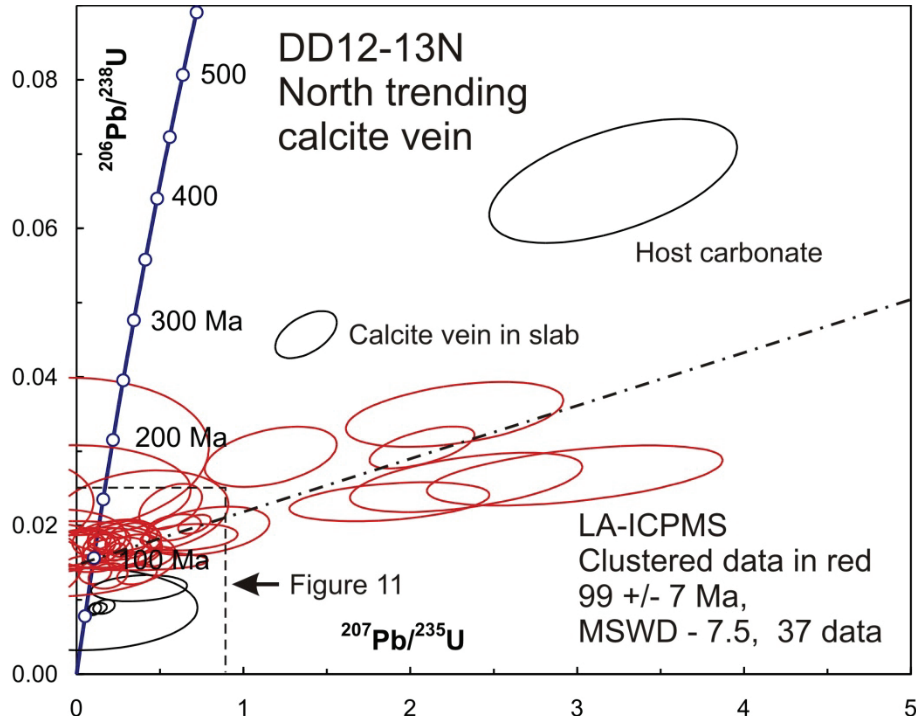

Figure 10: Concordia Diagram Showing All LA-ICPMS Data (n = 37) from North-trending Calcite Veins in Sample DD12-13N

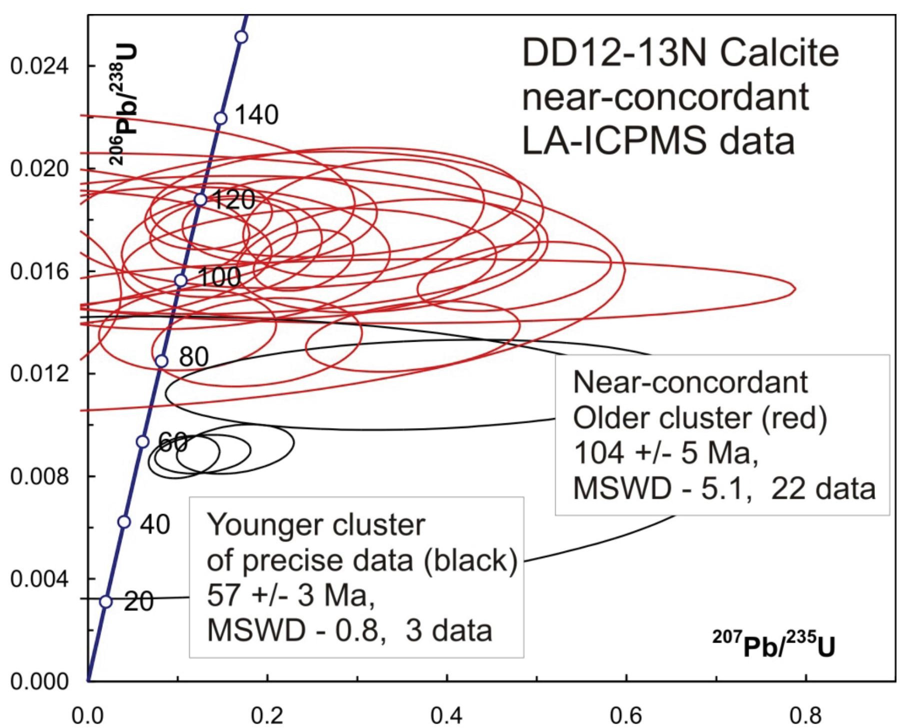

Figure 11: Concordia Diagram Showing Near-concordant LA-ICPMS Data from Sample DD12-13N (older cluster in red, n= 22, five younger analyses in black).

4.1.1.5 DGR-3-034.61 Drill Core (Devonian Lucas Formation)

Both calcite veins and limestone host material were targeted from available thin section material. Limestone host material has much higher U concentrations than vein material but Pb is significantly less radiogenic and the radiogenic component appears to have an older age (Figure 12). Dark, presumably organic-rich layers have the highest U content but Pb is the least radiogenic. A regression of all six data from the limestone gives a lower intercept age of 542 ± 110 Ma (MSWD – 7.7). Several analyses of the vein material are near-concordant but show a significant scatter of $^{206}Pb/^{238}U$ ages with a cluster around about 100 Ma but with four distinctly younger analyses extending down to 40 Ma (Figure 13).

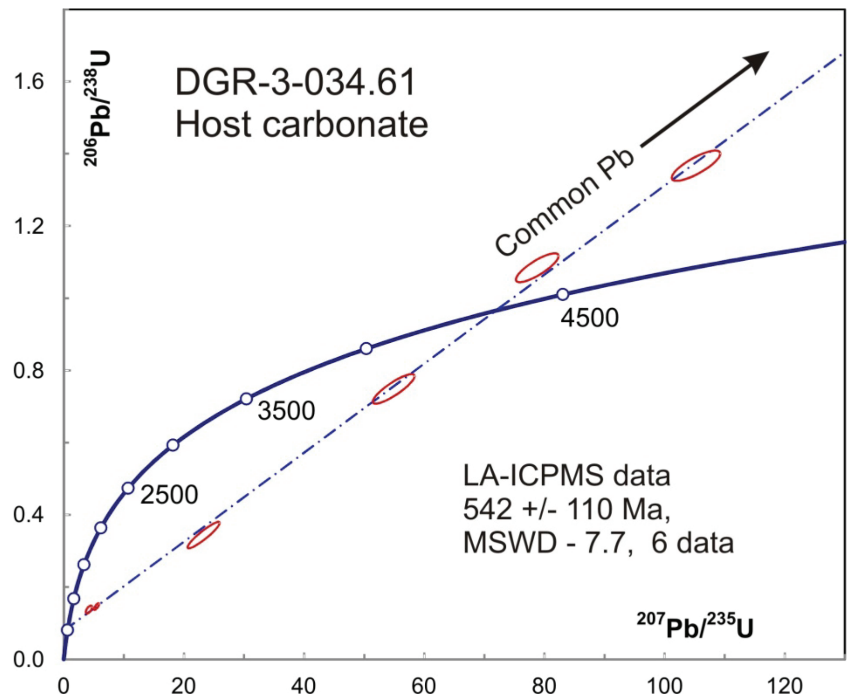

Figure 12: Concordia Diagram Showing LA-ICPMS Data (n = 6) from Carbonate that Hosts Veins in Sample DGR-3-034.61

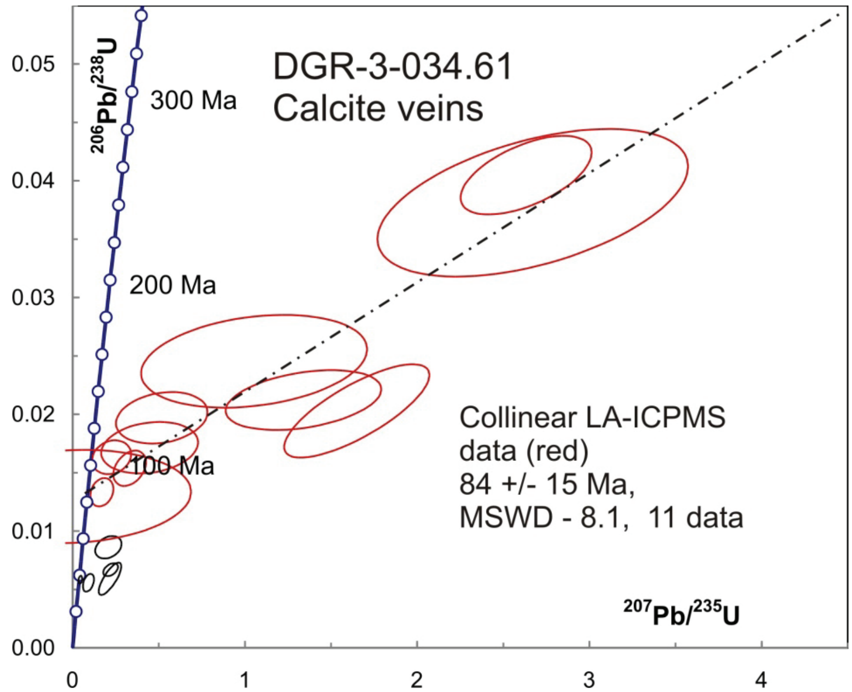

Figure 13: Concordia Diagram Showing LA-ICPMS Data (n = 11) from Calcite Veins in Sample DGR-3-034.61. Distinctly Younger Ellipses in Black are Omitted from the Regression

4.1.1.6 DGR-6-886.91B Drill Core (Ordovician Coboconk Formation)

Sample material from the Ordovician Coboconk Formation was collected from drill core at 887 m along the length of an inclined borehole which translates to approximately 776 m vertical depth. Only a small amount of vein material was left from this sample and U concentrations are much lower than in the surface and shallow samples. As in previous samples, Pb in the host rock is relatively unradiogenic (Figure 14) compared to that in the vein, which gave three near-concordant data with ages of around 450-550 Ma (Figure 15). Regressing 7 data, including one analysis from DGR-5-706.80 host carbonate, gives an age of 423 ± 77 Ma (Figure 14, MSWD – 7.8). Omitting one of the vein data gives a better fit with an age of 445 ± 42 Ma (Figure 15, MSWD – 1.7).

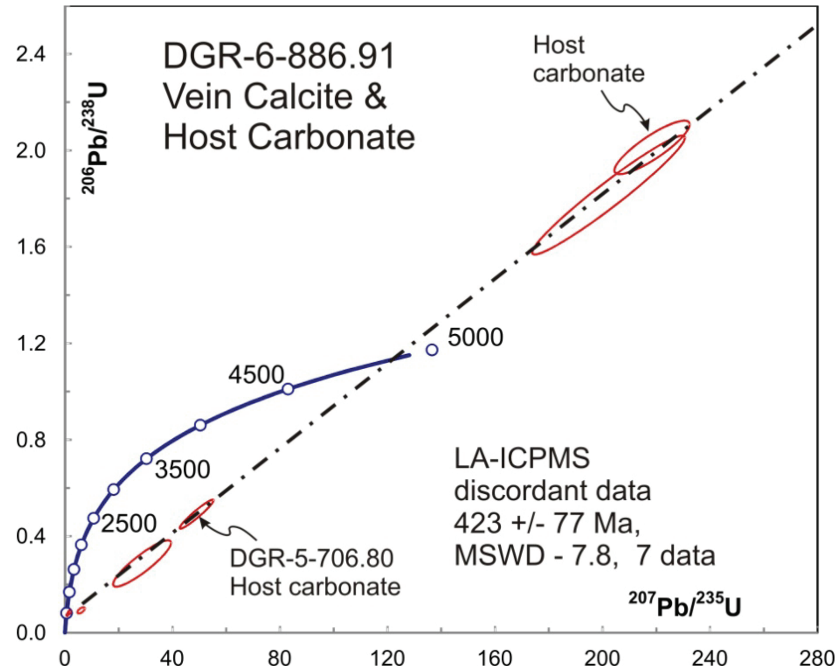

Figure 14: Concordia Diagram Showing Regression of Discordant LA-ICPMS Data (n = 6) from Vein Calcite and Host Carbonate. Six Discordant Data are from Sample DGR-6-886.91B and One from DGR-5-706.80.

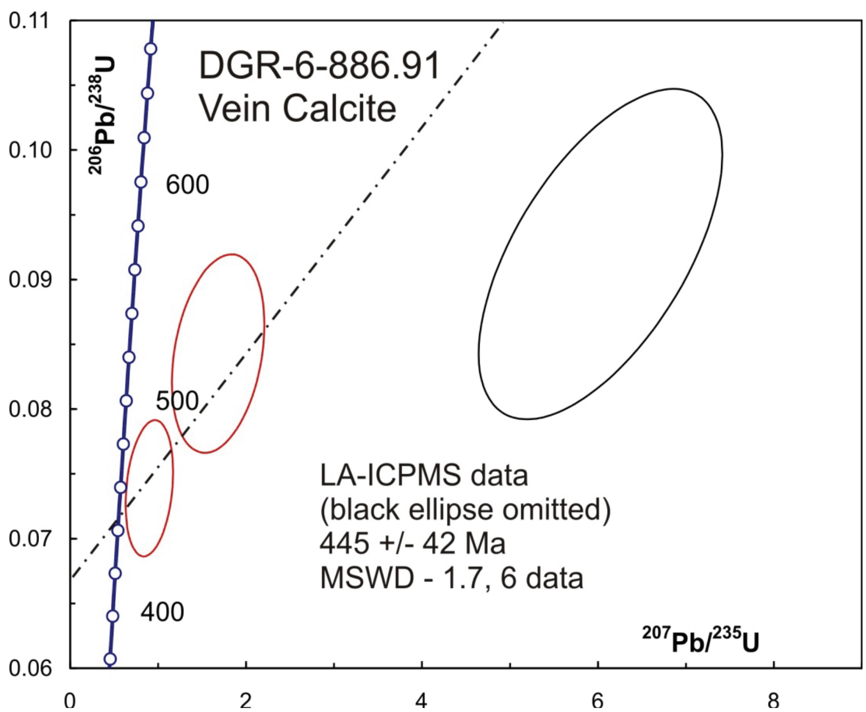

Figure 15: Concordia Diagram Showing Detail of Near-concordant LA-ICPMS Data from Calcite in Sample DGR-6-886.91B. Line is a Regression to the Two Red Ellipses and Four Highly Discordant Off-scale Data Shown in Figure 14 above.

4.2 ID-TIMS RESULTS

Calcite crystals showing the highest U and most radiogenic Pb analyses by LA-ICPMS were chosen for ID-TIMS dating, except for analysis DWD5776 (Table 3), which was chosen to provide an estimate of the initial common Pb isotopic composition. During analytical session 1, ID-TIMS analyses were carried out on thin section material of calcite crystals from the shallowest DGR vein (DGR-3-034.61) and two deep veins, DGR-5-706-80 and DGR-6-756.48B (results shown on left side of Figure 16). During analytical session 2, whole crystals from DD-12-11NE and DD12-12FV, were chosen. Only 9 analyses, including two aliquots of the same grain, are sufficiently radiogenic to be reliably plotted on a concordia curve. These results are shown on Figure 16 (right side), along with $^{206}Pb/^{238}U$ age results from the same grains by LA-ICPMS, where available.

Although the analyses are only moderately radiogenic (the proportion of measured ^{206}Pb that is non-radiogenic varied from 11% to 81%, as shown in Table 3 on page x), like those from the LA-ICPMS analyses , the data ellipses in Fig. 16 are concordant because they have been corrected for common Pb using the measured ^{204}Pb isotope, which cannot be done for LA-ICPMS. The fact that they are almost perfectly concordant, even for weakly radiogenic analyses like that from DGR-6-756, indicates that the Stacey and Kramers (1975) model common Pb chosen for correction is probably an accurate estimation of the common Pb component.

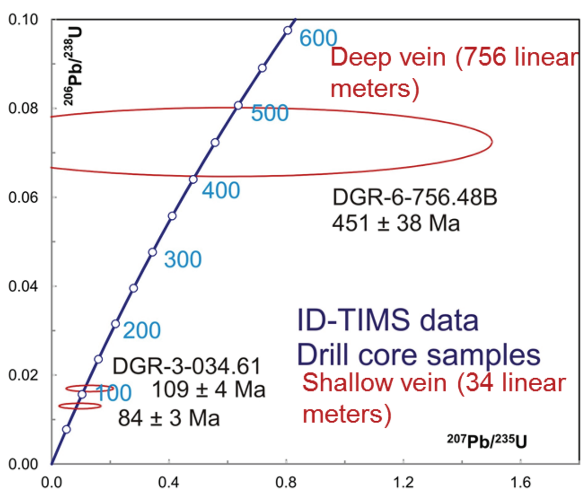

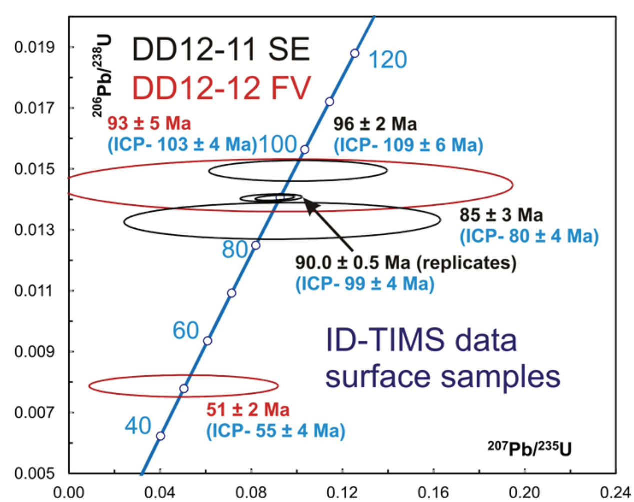

Figure 16: Concordia Diagrams Showing ID-TIMS Data from Calcite in Samples from Drill Core (left) and Surface (right). LA-ICPMS (ICP) Results are Shown for Corresponding Surface Samples

5. DISCUSSION

LA-ICPMS dating is relatively imprecise, with errors of about 5-10 million years, but allows material to be sampled at the 100 micron scale. ID-TIMS requires much larger samples but is more precise with errors of 1-2 million years or better on single analyses in favourable cases. The error ellipses measured by LA-ICPMS reflect the dispersion of ratios within the measured ablation profiles but the accuracy also depends on sample-standard reproducibility. This is normally a few percent for U-Pb analyses of zircon but in this case the NIST glass used as a standard has very different ablation properties than the calcite. Nevertheless, the ID-TIMS ages are comparable to LA-ICPMS ages on the same grains (e.g., right side of Figure 16). This suggests that LA-ICPMS is capable of producing reasonably accurate ages on calcite and that the age dispersion of radiogenic samples measured by LA-ICPMS reflects growth of calcite over an extended period of time. In particular, relatively young LA-ICPMS ages of ca. 50 Ma on some of the grains appear to be accurate so that at least two distinct pulses of calcite growth are reflected in the data.

There is no evidence that veins with different orientations from the Devonian bedrock have distinctly different ages, all show approximately the same span of ages. This is consistent with observations in the field and in cut slabs that veins do not crosscut each other but seem to fill a single fracture pattern within the host rock.

A frequency distribution of LA-ICPMS model $^{206}Pb/^{238}U$ ages (Table 2) from Devonian surface samples shows a broad peak extending from about 80 Ma to about 120 Ma, which tails off relatively slowly toward younger ages (Figure 17). This distribution is produced by adding up the normalized Gaussian curves representing errors for each LA-ICPMS datum. The fine-structure visible in the distribution is due to the presence of relatively precise data, which produce narrow, high gaussian curves. A significant peak is also present at around 52 Ma. The ca. 50 Ma spots are in some cases within samples that also gave ca. 100 Ma when measured at another spot.

Late Cretaceous to early Cenozoic-aged veins have only been found in the Devonian surface samples and in the shallow drill core at 35 vertical meters depth below ground surface. The calcite veins from deeper drill core in the Ordovician formations show much lower U concentrations and older Paleozoic ages that seem to approximate the age of the carbonate host rock. The results indicate that the fractures filled by these veins in the Ordovician rocks were most likely formed shortly after carbonate deposition from a fluid, possibly seawater, that was distinctly different from the groundwater responsible for deposition of the near-surface veins. No evidence has been found for an earlier (older) generation of veins in the near-surface samples nor has evidence been found for the Late Cretaceous to early Cenozoic veins in the deep samples.

The extended age range for emplacement of calcite vein material in the Lucas Formation is confirmed by the much less voluminous but more accurate ID-TIMS data. It appears that vein emplacement within shallow strata initially occurred at about 110-100 Ma. The duration of the main pulse of vein infill lasted tens of millions of years and was followed by a renewed pulse of fluid movement at about 50 Ma (Figure 15). It is possible that the fractures themselves are older than the infill material.

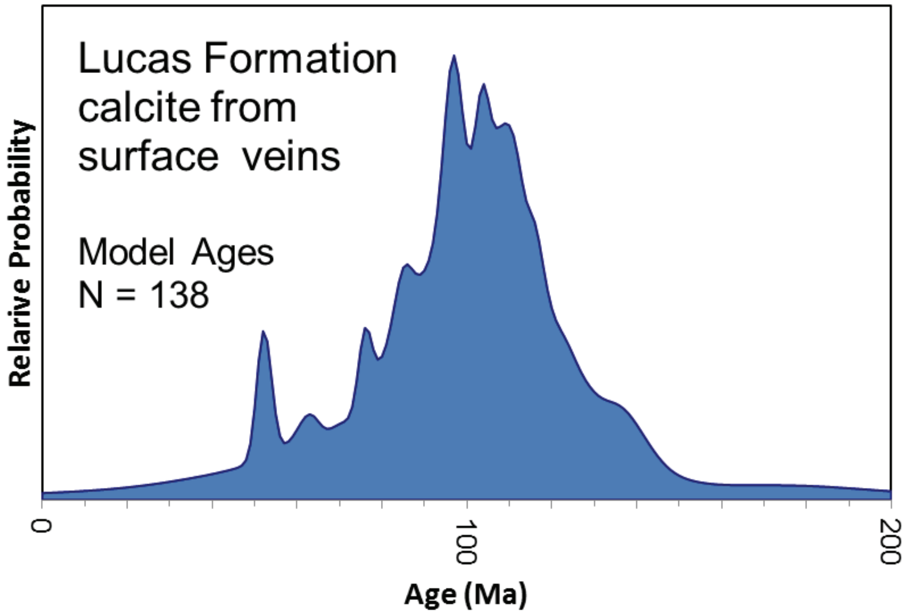

Figure 17: Probability Density Distribution for Model $^{206}Pb/^{238}U$ Ages from LA-ICPMS Analyses of Surface Calcite Vein Samples from the Devonian Lucas Formation

6. CONCLUSIONS

U levels are sufficiently high and initial common Pb levels low enough in vein calcite that useful ages can be determined by LA-ICPMS in favourable cases. Calcite in veins from the Devonian Lucas Formation is much younger than the host rock and appears to have crystallized over an extended period of time with an early pulse around 100 Ma and a later event around 50 Ma. Calcite from deeper veins in the Ordovician Coboconk Formation contains lower U concentrations and less radiogenic Pb but gives ages that are much closer to the depositional age of the host rocks. The comparability of ages yielded using the two methods (LA-ICPMS and ID-TIMS) supports the reliability of the results. No evidence is seen for more recent (e.g., Pleistocene) calcite growth in either the shallow Devonian or deep Ordovician calcite veins.

ACKNOWLEDGEMENTS

Support from the Natural Science and Engineering Research Council of Canada (NSERC) in the form of a Research Tools and Instruments (RTI) grant allowed the S-option sensitivity upgrade to the LA-ICPMS. Without this, much of the work in this report would not have been possible.

REFERENCES

Adams, J. and P.W. Basham. 1991. The seismicity and seismotectonics of eastern Canada. In: Slemmons, D.B. et al. (Eds.), Neotectonics of North America. Geological Society of America, Decade Map vol. 1, 261-275.

Armstrong, D.K. and T.R. Carter. 2010. The Subsurface Paleozoic Stratigraphy of Southern Ontario. Ontario Geological Survey, Special Volume 7.

Bailey Geological Services Ltd. and R.O. Cochrane. 1984a. Evaluation of the conventional and potential oil and gas reserves of the Cambrian of Ontario. Ontario Geological Survey, Open File Report 5499.

Bailey Geological Services Ltd. and R.O. Cochrane. 1984b. Evaluation of the conventional and potential oil and gas reserves of the Ordovician of Ontario. Ontario Geological Survey, Open File Report 5498.

Barnett, R.L., M. Arima, J.D. Blackwell, C.G. Winder, H.C. Palmer and A. Hayatsu. 1984. The Picton and Varty Lake ultramafic dikes: Jurassic magmatism in the St. Lawrence Platform near Belleville, Ontario. Canadian Journal of Earth Sciences 21, 1460–1472.

Coakley, B. and M. Gurnis. 1995. Far field tilting of Laurentia during the Ordovician and constraints on the evolution of a slab under an ancient continent, Journal of Geophysical Research 100, 6313-6327.

Coakley, B.J., G.C. Nadon, and H.F. Wang. 1994. Spatial variations in tectonic subsidence during Tippecanoe I in the Michigan Basin. Basin Research 6, 131-140.

Coniglio, M. and A.E. William-Jones. 1992. Diagenesis of Ordovician carbonates from the north-east Michigan Basin, Manitoulin Island area, Ontario: Evidence from petrography, stable isotopes and fluid inclusions. Sedimentology 39, 813-836.

Crough, S. 1981. Mesozoic hotspot epeirogeny in eastern North America, Geology 9, 2 6.

Cruden, A. 2011. Outcrop Fracture Mapping. Nuclear Waste Management Organization Report NWMO DGR-TR-2011-43 R000. Toronto, Canada.

Engelder, T. 1982. Is There a Genetic Relationship Between Selected Regional Joints and Contemporary Stress Within the Lithosphere of North America? Tectonics 1(2), 161 177.

Gordon, R.G., and D.M. Jurdy. 1986. Cenozoic Global Plate Motions, Journal of Geophysical Research 91, 12,389–12,406.

Heaman, L.M. and B.A. Kjarsgaard. 2000. Timing of eastern North American kimberlite magmatism. Continental extension of the Great Meteor Hotspot Track? Earth and Planetary Science Letters Journal 178, 253-268.

Howell, P.D. and B.A. van der Pluijm. 1990. Early history of the Michigan Basin: subsidence and Appalachian tectonics. Geology 18, 1195-1198.

Howell, P.D. and B.A. van der Pluijm. 1999. Structural sequences and styles of subsidence in the Michigan basin. Geological Society of America Bulletin 111, 974-991.

Huff, W.D., S.M. Bergstrom and D.R. Kolata. 1992. Gigantic Ordovician volcanic ash fall in North America and Europe: biological, tectonomagmatic, and event-stratigraphic significance. Geology 20, 875-878.

INTERA. 2011. Descriptive Geosphere Site Model. Intera Engineering Ltd. report for the Nuclear Waste Management Organization NWMO DGR-TR-2011-24 R000. Toronto, Canada.

Jaffey, A.H., K.F. Flynn, L.E. Glendenin, W.C. Bentley and A.M. Essling. 1971. Precision measurement of half-lives and specific activities of 235U and 238U. Physical Review, 4: 1889-1906.

Johnson, M.D., D.K. Armstrong, B.V. Sanford, P.G. Telford and M.A. Rutka. 1992. Paleozoic and Mesozoic geology of Ontario. In: The Geology of Ontario, Ontario Geological Survey, Special Volume 4, Part 2, 907-1008.

Kolata, D.R., W.D. Huff and S.M. Bergström. 1998. Nature and regional significance of unconformities associated with the Middle Ordovician Hagan K-bentonite complex in the North American midcontinent. Geological Society of America Bulletin 110, 723-739.

Kumarapeli, P.S. and V.A. Saul. 1966. The St. Lawrence Rift Valley System. A North American Equivalent of the East African Rift Valley System. Canadian Journal of Earth Sciences 3, 639-658.

Legall, F.D., C.R. Barnes and R.W. Macqueen. 1981. Thermal maturation, burial history and hotspot development, Paleozoic strata of southern Ontario-Quebec, from conodont acritarch colour alteration studies. Bulletin of Canadian Petroleum Geology 29, 492-539.

Leighton, M.W. 1996. Interior cratonic basins: a record of regional tectonic influences. In: van der Pluijm, B.A. & Catacosinos, P.A. (Eds.), Basement and Basins of North America, Geological Society of America Special Paper 308, 77-93.

Lindholm, R.C. 1978. Triassic-Jurassic faulting in eastern North America – A model based on pre-Triassic structures. Geology 6, 365-368.

Ludwig, K.R. 2003. User's manual for Isoplot 3.00 a geochronological toolkit for Excel. Berkeley Geochronological Center Special Publication, 4, 71 p.

McFall, G.H. and A. Allam. 1989. Neotectonic Investigations in Southern Ontario. Prince Edward County, Phase I. Atomic Energy Control Board Report 89-02. Ottawa, Ontario.

McHone, J.G. 1996. Broad-terrane Jurassic flood basalts across northeastern North America. Geology 24, 319-322.

McHone, J.G. and J.R. Butler. 1984. Mesozoic igneous provinces of New England and the opening of the North Atlantic Ocean. Geological Society of America Bulletin 95, 757-765.

Minster, J. and T. Jordan. 1978. Present Day Plate Motions. Journal of Geophysical Research 83, 5331 5354.

Morgan, P. 1983. Constraints on rift thermal processes from heat flow and uplift. Tectonophysics 94, 277-298.

Münsterer, C. et al., 2011 Ion Beam Physics, ETH Zurich Annual Report, p 26.

Nadon G.C., J.A. Simo, R.H. Dott and C.W. Byers. 2000. High-resolution sequence stratigraphic analysis of the St. Peter Sandstone and Glenwood Formation (Middle Ordovician), Michigan Basin, U.S.A. AAPG Bulletin 84, 975-996.

NWMO. 2011. Geosynthesis. Nuclear Waste Management Organization Report NWMO DGR-TR-2011-11 R000. Toronto, Canada.

Quinlan, G. and C. Beaumont. 1984. Appalachian thrusting, lithospheric flexure and the Paleozoic stratigraphy of the Eastern Interior of North America. Canadian Journal of Earth Sciences 21, 973-996.

Rona, P.A. and E.S. Richardson. 1978. Early Cenozoic global plate reorganization. Earth and Planetary Science Letters 40, 1-11.

Sanford, B.V., F.J. Thompson and G.H. McFall. 1985. Plate tectonics – A possible controlling mechanism in the development of hydrocarbon traps in southwestern Ontario. Bulletin of Canadian Petroleum Geology 33, 52-71.

Sbar, M.L. and L.R. Sykes. 1973. Contemporary Compressive Stress and Seismicity in Eastern North America: An Example of Intra-Plate Tectonics. Geological Society of America Bulletin 84, 1861-1882.

Stacey, J.S. and J.D. Kramers. 1975. Approximation of terrestrial lead isotope evolution by a two-stage model. Earth and Planetary Science Letters, 26(2): 207-221.

Thomas, W.A. 2006. Tectonic inheritance at a continental margin. GSA Today 16(2), 4-11.

Uyeno, T.T., P.G. Telford and B.V. Sanford. 1982. Devonian conodonts and stratigraphy of southwestern Ontario. Geological Survey of Canada, Bulletin 332.

Wang, H.F., K.D. Crowley and G.C. Nadon. 1994. Thermal History of the Michigan Basin from Apatite Fission-Track Analysis and Vitrinite Reflectance. In Basin Compartments and Seals, P. J. Ortoleva (Ed.), AAPG Memoir 61, 167-178.

Wheeler, R.L. 1995. Earthquakes and the cratonward limit of Iapetan faulting in eastern North America. Geology 23, 105-108.

Williams, H. and R.D. Hatcher. 1982. Suspect terranes and accretionary history of the Appalachian Orogen. Geology 10, 530-536.

Zoback, M.L. and M.D. Zoback. 1989. Regional tectonic stress field of the continental U.S. Geophysical Framework of the Continental U.S. Pakiser, L. and W.D. Mooney (Eds.), Geological Society of America Memoir 172, 523-539.

Table 2: LA-ICPMS U-Pb Isotopic Data from Vein Calcite in Carbonate Collected from the Area of the Bruce Nuclear Site

	Spot	U (ppm)	Pb^{206} (ppm)	Th / U	$^{207}Pb/^{235}U$	1 Sig	$^{206}Pb/^{238}U$	1 Sig	Error Correl.	$^{207}Pb/^{235}U$ Age (Ma)	1 Sig	$^{206}Pb/^{238}U$ Age (Ma)	1 Sig	$^{206}Pb/^{238}U$ Model Age (Ma)	1 Sig
	DD12-11NE vein set														
1	DD12-11-1.1	1.5	0.25	0.01	0.336	0.045	0.0171	0.0006	0.25131	294	34	109	4	96	3
2	DD12-11-2.1	1.8	0.31	0.01	0.138	0.025	0.0171	0.0005	0.16414	131	22	109	3	108	2
3	DD12-11-3B.1	2.1	0.32	0.01	0.103	0.022	0.0151	0.0004	0.14113	100	20	97	3	97	2
4	DD12-11-4.1	0.7	0.16	0.06	0.327	0.059	0.0216	0.0009	0.22925	287	44	138	6	127	4
5	DD12-11-5.1	1.1	0.28	0.01	1.817	0.116	0.0265	0.0010	0.56167	1052	41	169	6	72	7
6	DD12-11-6.1	5.1	0.79	0.02	0.140	0.011	0.0154	0.0003	0.28672	133	10	99	2	97	2
7	DD12-11-6.2	1.6	0.27	0.01	0.301	0.039	0.0170	0.0005	0.22347	268	30	109	3	98	3
8	DD12-11-7.1	0.7	0.13	0.03	0.586	0.066	0.0186	0.0009	0.43073	468	42	119	6	92	4
9	DD12-11-8.1	2.4	0.42	0.01	0.284	0.033	0.0180	0.0006	0.26778	254	26	115	4	105	3
10	DD12-11-9.1	1.6	0.26	0.02	0.205	0.027	0.0161	0.0006	0.27254	189	22	103	4	97	3
11	DD12-11-9.2	1.7	0.28	0.00	0.237	0.029	0.0162	0.0005	0.23701	216	24	104	3	96	2
12	DD12-11-10.1	1.6	0.27	0.01	0.263	0.029	0.0173	0.0007	0.34259	237	23	110	4	102	3
13	DD12-11-11.1	1.5	0.23	0.02	0.258	0.031	0.0156	0.0006	0.34080	233	24	100	4	91	3
14	DD12-11-12.1	2.6	0.33	0.01	0.158	0.015	0.0125	0.0003	0.26827	149	13	80	2	76	2
15	DD12-11-13.1	1.8	0.44	0.01	1.452	0.134	0.0237	0.0008	0.38520	911	54	151	5	75	8
16	DD12-11-14.1	3.4	0.46	0.06	0.153	0.013	0.0139	0.0004	0.31633	145	12	89	2	85	2
17	DD12-11-15.1	1.3	0.21	0.01	0.211	0.044	0.0158	0.0007	0.20162	195	36	101	4	95	3
18	DD12-11-16.1	2.7	0.42	0.01	0.162	0.015	0.0158	0.0004	0.28551	152	13	101	3	97	2
19	DD12-11-17.1	1.7	0.29	0.01	0.235	0.029	0.0164	0.0005	0.24909	214	24	105	3	98	2
20	DD12-11-18.1	0.9	0.23	0.02	0.697	0.099	0.0245	0.0015	0.42179	537	58	156	9	125	7
21	DD12-11-19.1	1.4	0.23	0.01	0.174	0.027	0.0162	0.0005	0.20518	163	23	104	3	100	2
22	DD12-11-20.1	0.6	0.11	0.03	0.454	0.096	0.0177	0.0008	0.22441	380	65	113	5	94	6
23	DD12-11-21.1	1.8	0.32	0.02	0.195	0.022	0.0177	0.0005	0.27129	181	19	113	3	109	3
24	DD12-11-22.1	1.0	0.12	0.02	0.402	0.050	0.0124	0.0006	0.40290	343	36	79	4	60	3
25	DD12-11-24.1	0.9	0.16	0.02	0.554	0.052	0.0181	0.0007	0.43455	447	34	115	5	90	4
26	DD12-11-3.1	0.1	0.05	0.03	4.046	0.724	0.0342	0.0027	0.43281	1644	138	217	17	-8	50
27	DD12-11-3.2	0.3	0.07	0.01	2.556	0.518	0.0253	0.0016	0.31337	1288	139	161	10	20	37

	Spot	U	Pb^{206}	Th	^{207}Pb	1	^{206}Pb	1	Error	^{207}Pb	1	^{206}Pb	1	^{206}Pb	1
		(ppm)	(ppm)	U	^{235}U	Sig	^{238}U	Sig	Correl.	^{235}U	Sig	^{238}U	Sig	^{238}U	Sig
										Age (Ma)		Age (Ma)		Model Age (Ma)	
28	DD12-11-3.4	0.3	0.07	0.02	2.031	0.408	0.0264	0.0016	0.29589	1126	129	168	10	59	28
29	DD12-11-3.5	0.3	0.36	0.02	11.733	0.703	0.1174	0.0054	0.77219	2583	55	716	31	101	42
30	DD12-11-3.8	0.5	0.10	0.01	0.905	0.169	0.0185	0.0009	0.27492	655	86	118	6	72	11
31	DD12-11-3.9	0.3	0.07	0.02	2.029	0.425	0.0262	0.0014	0.26195	1125	134	167	9	58	30
32	DD12-11-3.10	0.6	0.10	0.01	1.032	0.192	0.0171	0.0009	0.28330	720	92	109	6	55	13
33	DD12-11-3.11	0.4	0.09	0.01	1.509	0.221	0.0206	0.0011	0.34866	934	86	132	7	51	14
	DD12-12SE vein set														
34	DD12-12-1.1	1.0	0.21	0.03	-0.040	0.055	0.0204	0.0009	0.01000	-42	57	130	6	141	4
35	DD12-12-2.1	3.4	0.61	0.01	0.189	0.014	0.0182	0.0003	0.25985	176	11	116	2	112	2
36	DD12-12-3.1	1.4	0.23	0.03	0.139	0.028	0.0170	0.0005	0.15750	132	25	109	3	107	3
37	DD12-12-4.1	2.8	0.46	0.01	0.134	0.016	0.0166	0.0003	0.17186	128	14	106	2	105	2
38	DD12-12-5.1	1.1	0.26	0.01	0.900	0.104	0.0247	0.0012	0.43440	652	54	158	8	115	7
39	DD12-12-6.1	3.1	0.52	0.02	0.180	0.021	0.0167	0.0003	0.17815	168	18	107	2	103	2
40	DD12-12-7.1	0.7	0.14	0.05	0.404	0.069	0.0192	0.0009	0.26649	345	48	122	5	106	4
41	DD12-12-8.1	1.4	0.26	0.15	0.175	0.025	0.0178	0.0004	0.17283	163	21	114	3	111	2
42	DD12-12-8.2	0.4	0.08	0.10	0.321	0.111	0.0189	0.0010	0.14502	282	82	121	6	109	7
43	DD12-12-9.1	1.8	0.34	0.02	0.213	0.023	0.0188	0.0006	0.31009	196	19	120	4	115	3
44	DD12-12-10.1	1.9	0.38	0.04	0.225	0.024	0.0200	0.0005	0.25026	206	20	128	3	122	3
45	DD12-12-11.1	1.7	0.26	0.03	0.336	0.036	0.0153	0.0005	0.27440	294	27	98	3	84	2
46	DD12-12-12.1	2.7	0.49	0.02	0.355	0.036	0.0183	0.0004	0.22974	308	27	117	3	103	2
47	DD12-12-12.2	0.3	0.08	0.12	0.771	0.147	0.0272	0.0018	0.34030	580	82	173	11	139	9
48	DD12-12-13.1	1.7	0.39	0.02	0.269	0.030	0.0224	0.0007	0.29058	242	24	143	5	136	4
49	DD12-12-14.1	1.5	0.28	0.03	0.210	0.025	0.0183	0.0005	0.22649	194	21	117	3	112	2
50	DD12-12-15.1	2.6	0.52	0.02	0.498	0.057	0.0200	0.0005	0.23520	410	38	127	3	106	3
51	DD12-12-16.1	4.3	0.59	0.03	0.301	0.018	0.0138	0.0003	0.36563	267	14	89	2	76	1
52	DD12-12-16.2	0.8	0.15	0.02	0.300	0.048	0.0197	0.0007	0.22300	266	37	125	4	116	3
53	DD12-12-17.1	0.2	0.07	0.28	1.566	0.272	0.0300	0.0022	0.41658	957	103	191	14	111	16
54	DD12-12-19.1	3.0	0.49	0.02	0.168	0.015	0.0165	0.0003	0.23220	158	13	106	2	102	2
55	DD12-12-20.1	4.5	0.87	0.02	0.373	0.033	0.0193	0.0005	0.27431	322	24	123	3	109	2
56	DD12-12-21.1	1.2	0.21	0.04	0.182	0.033	0.0174	0.0006	0.18150	170	28	111	4	107	3

	Spot	U	Pb^{206}	Th	^{207}Pb	1	^{206}Pb	1	Error	^{207}Pb	1	^{206}Pb	1	^{206}Pb	1
		(ppm)	(ppm)	U	^{235}U	Sig	^{238}U	Sig	Correl.	^{235}U	Sig	^{238}U	Sig	^{238}U	Sig
										Age (Ma)		Age (Ma)		Model Age (Ma)	
57	DD12-12-22.1	0.8	0.15	0.00	0.389	0.061	0.0204	0.0010	0.30483	334	44	130	6	115	5
	DD12-12FV flat veins														
58	DD12-12-1.1	1.6	0.14	0.03	-0.040	0.030	0.0090	0.0005	0.01000	-42	31	57	3	63	2
59	DD12-12-1.2	0.4	0.09	0.06	0.389	0.171	0.0206	0.0013	0.13776	333	118	131	8	117	10
60	DD12-12-1.3	1.2	0.17	0.08	0.125	0.040	0.0145	0.0005	0.11300	120	36	93	3	91	3
61	DD12-12-2.1	1.1	0.17	0.01	0.112	0.034	0.0154	0.0007	0.13898	108	31	98	4	98	3
62	DD12-12-2.2	0.9	0.15	0.02	0.664	0.075	0.0182	0.0008	0.39698	517	45	116	5	84	5
63	DD12-12-3.1	0.4	0.19	0.02	3.384	0.451	0.0446	0.0030	0.51333	1501	101	281	19	102	27
64	DD12-12-3.2	3.3	0.59	0.01	0.127	0.017	0.0182	0.0003	0.14301	122	15	116	2	116	2
65	DD12-12-3.3	0.5	0.11	0.03	0.851	0.263	0.0247	0.0019	0.25200	625	136	157	12	117	16
66	DD12-12-3.4	0.8	0.12	0.02	0.166	0.072	0.0157	0.0009	0.13338	156	61	100	6	97	5
67	DD12-12-3.5	0.9	0.20	0.02	1.006	0.147	0.0212	0.0010	0.30815	707	72	135	6	84	9
68	DD12-12-4.1	0.4	0.13	0.06	1.544	0.235	0.0294	0.0017	0.37705	948	90	187	11	108	14
69	DD12-12-4.2	1.2	0.28	0.03	1.167	0.116	0.0231	0.0009	0.41299	785	53	147	6	88	7
70	DD12-12-4.3	1.0	0.14	0.01	0.113	0.060	0.0138	0.0006	0.07950	108	53	89	4	87	4
71	DD12-12-5.1	0.4	0.09	0.05	0.612	0.249	0.0240	0.0017	0.17460	485	146	153	11	126	15
72	DD12-12-5.2	0.7	0.15	0.16	0.256	0.078	0.0206	0.0010	0.15497	231	61	132	6	125	5
73	DD12-12-5.3	0.5	0.09	0.04	0.259	0.139	0.0187	0.0016	0.16003	234	106	120	10	112	9
74	DD12-12-7.1	0.7	0.13	0.06	0.003	0.082	0.0202	0.0010	0.00155	3	80	129	6	137	5
75	DD12-12-7.2	0.4	0.08	0.07	0.168	0.211	0.0187	0.0017	0.07131	158	168	119	11	117	12
76	DD12-12-1.1	0.8	0.10	0.00	0.075	0.232	0.0126	0.0015	0.03960	74	199	81	10	81	14
77	DD12-12-2.1	0.3	0.06	0.09	0.545	0.441	0.0199	0.0020	0.12273	442	256	127	12	103	29
78	DD12-12-2.2	0.6	0.14	0.04	1.693	0.304	0.0213	0.0011	0.27544	1006	109	136	7	45	21
79	DD12-12-3.1	0.4	0.13	0.17	1.882	0.369	0.0286	0.0021	0.37303	1075	123	182	13	83	23
80	DD12-12-4.1	0.6	0.28	0.06	2.853	0.493	0.0465	0.0044	0.54824	1370	124	293	27	146	29
81	DD12-12-4.2	1.5	0.44	0.02	1.484	0.215	0.0292	0.0014	0.33772	924	85	185	9	110	13
82	DD12-12-5.1	0.8	0.39	0.05	2.928	0.537	0.0521	0.0051	0.53475	1389	132	327	31	179	32
83	DD12-12-6.1	1.7	0.33	0.02	0.206	0.027	0.0191	0.0004	0.17821	190	22	122	3	118	2
84	DD12-12-7.1	0.6	0.25	0.00	2.169	0.315	0.0400	0.0028	0.48175	1171	97	253	17	143	19
85	DD12-12-8.1	0.3	0.07	0.00	0.963	0.279	0.0252	0.0019	0.26490	685	136	160	12	114	17
86	DD12-12-9.1	0.6	0.14	0.03	0.789	0.127	0.0210	0.0010	0.28287	591	70	134	6	96	8

	Spot	U	Pb206	Th	^{207}Pb	1	^{206}Pb	1	Error	^{207}Pb	1	^{206}Pb	1	^{206}Pb	1
		(ppm)	(ppm)	U	^{235}U	Sig	^{238}U	Sig	Correl.	^{235}U	Sig	^{238}U	Sig	^{238}U	Sig
										Age (Ma)		Age (Ma)		Model Age (Ma)	
87	DD12-12-10.1	0.4	0.10	0.35	3.754	1.634	0.0259	0.0029	0.25266	1583	304	165	18	-47	126
88	DD12-12-10.2	2.6	1.20	0.01	3.101	0.147	0.0456	0.0012	0.56008	1433	36	287	7	125	9
89	DD12-12-11.1	1.2	0.26	0.00	0.535	0.080	0.0221	0.0011	0.32788	435	52	141	7	118	5
90	DD12-12-12.1	1.2	0.19	0.04	0.143	0.050	0.0152	0.0008	0.14327	136	43	97	5	95	4
91	DD12-12-13.1	0.4	0.32	0.07	5.442	0.478	0.0735	0.0037	0.56921	1891	73	457	22	175	28
92	DD12-12-14.1	0.4	0.21	0.07	4.791	0.738	0.0540	0.0040	0.48658	1783	123	339	25	82	47
93	DD12-12-14.2	1.5	0.80	0.02	4.148	0.180	0.0547	0.0013	0.56672	1664	35	343	8	125	11
94	DD12-12-15.1	1.6	0.29	0.09	0.363	0.043	0.0182	0.0007	0.32601	315	31	116	4	102	3
95	DD12-12-16.1	5.6	0.93	0.01	0.132	0.010	0.0164	0.0003	0.22021	126	9	105	2	104	1
96	DD12-12-17.1	0.3	0.09	0.14	-0.910	0.718	0.0307	0.0029	0.01000	-2443	3546	195	18	260	48
97	DD12-12-18.1	0.4	0.12	0.00	1.542	0.498	0.0292	0.0027	0.28716	947	183	185	17	107	31
98	DD12-12-19.1	1.9	0.53	0.02	1.753	0.077	0.0276	0.0007	0.56046	1028	28	175	4	83	5
99	DD12-12-20.1	1.5	0.22	0.02	0.256	0.041	0.0148	0.0005	0.22953	232	32	95	3	86	3
100	DD12-12-21.1	3.6	0.31	0.01	0.113	0.017	0.0085	0.0003	0.21252	108	15	55	2	51	1
	DD12-13N vein set														
101	DD12-13-1.1	0.7	0.22	0.02	2.071	0.129	0.0305	0.0012	0.60852	1139	42	194	7	84	8
102	DD12-13-1.2	0.5	0.12	0.03	1.875	0.245	0.0232	0.0011	0.35380	1072	84	148	7	46	16
103	DD12-13-2.1	2.1	0.35	0.01	0.240	0.023	0.0164	0.0005	0.31274	219	18	105	3	97	2
104	DD12-13-2.2	0.4	0.09	0.05	0.775	0.156	0.0193	0.0013	0.34515	583	86	123	8	85	9
105	DD12-13-3.1	3.6	0.32	0.00	0.107	0.016	0.0088	0.0003	0.25627	103	15	56	2	53	2
106	DD12-13-3.2	0.8	0.14	0.02	0.307	0.055	0.0181	0.0009	0.28954	272	42	115	6	104	4
107	DD12-13-4.1	1.3	0.23	0.02	0.151	0.033	0.0175	0.0006	0.14373	143	29	112	4	109	3
108	DD12-13-4.2	1.6	0.26	0.01	0.475	0.044	0.0158	0.0006	0.37646	395	30	101	4	79	3
109	DD12-13-5.1	0.3	0.07	0.00	2.987	0.363	0.0267	0.0017	0.50909	1404	89	170	10	4	24
110	DD12-13-5.2	0.3	0.11	0.00	2.266	0.266	0.0350	0.0018	0.43570	1202	80	222	11	103	16
111	DD12-13-6.1	0.9	0.12	0.00	0.111	0.040	0.0137	0.0006	0.12918	107	36	88	4	87	3
112	DD12-13-6.2	0.1	0.03	0.12	-0.020	0.288	0.0248	0.0025	0.01000	-20	261	158	16	169	17
113	DD12-13-7.1	2.4	0.21	0.01	0.128	0.022	0.0089	0.0003	0.20494	122	19	57	2	53	2
114	DD12-13-8.2	0.9	0.17	0.00	0.214	0.044	0.0180	0.0007	0.18113	197	36	115	4	109	3
115	DD12-13-9.1	0.8	0.14	0.22	0.149	0.046	0.0170	0.0008	0.15559	141	40	108	5	106	4
116	DD12-13-9.2	0.8	0.19	0.00	0.563	0.077	0.0226	0.0013	0.40766	453	49	144	8	120	6

	Spot	U	Pb^{206}	Th	^{207}Pb	1	^{206}Pb	1	Error	^{207}Pb	1	^{206}Pb	1	^{206}Pb	1
		(ppm)	(ppm)	U	^{235}U	Sig	^{238}U	Sig	Correl.	^{235}U	Sig	^{238}U	Sig	^{238}U	Sig
										Age (Ma)		Age (Ma)		Model Age (Ma)	
117	DD12-13-10.1	0.6	0.11	0.04	0.277	0.085	0.0187	0.0009	0.15254	248	65	119	6	110	5
118	DD12-13-11.2	0.4	0.11	0.00	2.335	0.285	0.0258	0.0016	0.51821	1223	84	164	10	37	18
119	DD12-13-12.1	0.3	0.09	0.06	1.164	0.162	0.0293	0.0017	0.40733	784	74	186	10	129	10
120	DD12-13-12.2	3.6	0.54	0.01	0.366	0.173	0.0152	0.0005	0.07117	317	121	97	3	82	12
121	DD12-13-1A.1	0.3	0.05	0.04	-0.245	0.115	0.0147	0.0019	0.10000	-286	146	94	12	114	9
122	DD12-13-1B.1	0.3	0.06	0.12	-0.156	0.185	0.0183	0.0016	0.10000	-172	201	117	10	133	11
123	DD12-13-2.1	0.3	0.08	0.02	-0.483	0.239	0.0226	0.0028	0.10000	-670	396	144	17	181	15
124	DD12-13-4.1	0.7	0.13	0.00	0.241	0.109	0.0180	0.0011	0.13358	219	86	115	7	108	6
125	DD12-13-4.2	0.6	0.10	0.01	-0.093	0.122	0.0165	0.0011	0.10000	-99	128	105	7	117	7
126	DD12-13-5.1	0.5	0.09	0.01	0.142	0.148	0.0170	0.0011	0.06211	135	124	109	7	107	9
127	DD12-13-5.2	0.6	0.10	0.02	0.095	0.099	0.0165	0.0011	0.06586	92	88	106	7	106	6
128	DD12-13-5.3	0.8	0.09	0.00	0.375	0.118	0.0116	0.0007	0.19758	324	84	74	5	56	7
129	DD12-13-5.4	0.7	0.06	0.05	0.042	0.279	0.0087	0.0023	0.03867	42	241	56	14	57	17
130	DD12-13-3.1	0.3	0.07	0.06	0.389	0.213	0.0218	0.0023	0.19238	334	145	139	14	125	13
131	DD12-13-3.2	1.6	0.31	0.01	0.582	0.067	0.0197	0.0007	0.31974	466	42	126	5	99	4
132	DD12-13-6.1	0.9	0.14	0.01	0.339	0.071	0.0166	0.0009	0.25983	296	52	106	6	93	5
133	DD12-13-6.3	1.4	0.26	0.02	0.674	0.119	0.0184	0.0007	0.22255	523	70	118	5	85	7
134	DD12-13-6.4	1.6	0.33	0.01	0.706	0.040	0.0202	0.0005	0.45725	543	24	129	3	95	3
135	DD12-13-6.5	1.3	0.18	0.01	0.362	0.049	0.0134	0.0006	0.31032	314	36	86	4	70	3
136	DD12-13-7.1	0.5	0.08	0.02	-0.251	0.176	0.0171	0.0013	0.10000	-294	215	109	8	131	10
137	DD12-13-8.1	2.0	0.18	0.00	0.164	0.027	0.0091	0.0004	0.26682	154	23	58	3	52	2
138	DD12-13-9.1	1.7	0.31	0.00	0.134	0.029	0.0181	0.0005	0.13504	128	26	116	3	115	3
139	DD12-13-10.1	0.2	0.05	0.06	-0.144	0.383	0.0294	0.0043	0.10000	-157	375	187	27	207	23
140	DD12-13-11.1	0.9	0.14	0.00	0.247	0.085	0.0163	0.0009	0.15594	224	67	104	6	96	5
141	DD12-13-11.2	0.3	0.04	0.00	-0.081	0.278	0.0155	0.0021	0.10000	-86	268	99	13	110	17
142	DD12-13-Vein.1	2.1	0.97	0.02	1.375	0.075	0.0457	0.0013	0.51707	878	32	288	8	227	6
143	DD12-13-Host.1 lmst	0.6	0.40	0.04	3.216	0.303	0.0664	0.0034	0.54487	1461	71	414	21	258	18
144	DD12-13-5.5c	1.1	0.14	0.00	0.188	0.048	0.0132	0.0007	0.20967	175	40	85	4	79	3
	DGR-3-034.61 Drill core														
145	DGR-3-1.1	1.09	0.01	0.04	0.217	0.027	0.0059	0.0006	0.77508	199	22	38	4	27	3
146	DGR-3-1.2	0.24	0.01	0.17	0.331	0.039	0.0154	0.0006	0.34363	290	29	98	4	85	3

	Spot	U	Pb^{206}	Th	^{207}Pb	1	^{206}Pb	1	Error	^{207}Pb	1	^{206}Pb	1	^{206}Pb	1
		(ppm)	(ppm)	U	^{235}U	Sig	^{238}U	Sig	Correl.	^{235}U	Sig	^{238}U	Sig	^{238}U	Sig
										Age (Ma)		Age (Ma)		Model Age (Ma)	
147	DGR-3-1.3	1.03	0.01	0.05	0.091	0.013	0.0056	0.0003	0.39011	89	12	36	2	33	2
148	DGR-3-2.1	1.11	0.01	0.05	0.220	0.018	0.0067	0.0002	0.42387	202	15	43	1	32	1
149	DGR-3-3.1	0.50	0.01	0.10	0.169	0.027	0.0133	0.0005	0.22867	159	24	85	3	81	2
150	DGR-3-3.2	0.17	0.01	0.20	0.517	0.108	0.0197	0.0009	0.21813	423	70	126	6	103	6
151	DGR-3-3.3	0.29	0.01	0.13	0.226	0.046	0.0163	0.0006	0.17823	207	38	104	4	97	3
152	DGR-3-4.1	0.31	0.03	0.14	2.632	0.156	0.0405	0.0014	0.57472	1310	43	256	9	119	9
153	DGR-3-4.2	1.38	0.83	0.16	24.547	1.476	0.3003	0.0147	0.81531	3290	58	1693	73	570	85
154	DGR-3-5.1	0.47	0.01	0.14	0.207	0.031	0.0086	0.0004	0.30313	191	26	55	3	46	2
155	DGR-3-6.1	3.30	0.04	0.09	0.044	0.004	0.0058	0.0001	0.24572	44	4	38	1	37	1
156	DGR-3-6.2	2.13	0.09	0.05	1.650	0.172	0.0203	0.0016	0.77073	989	65	129	10	40	10
157	DGR-3-7.1 br lmst	3.08	0.90	0.03	5.464	0.178	0.1460	0.0037	0.78293	1895	28	878	21	650	17
158	DGR-3-8.1 bk lmst	10.05	21.79	0.03	78.820	1.451	1.0840	0.0163	0.81801	4447	18	4734	51	2624	108
159	DGR-3-9.1 bk lmst	3.97	5.95	0.03	54.916	1.420	0.7486	0.0167	0.86309	4086	26	3602	61	1731	84
160	DGR-3-9.2 br lmst	3.03	0.83	0.03	4.203	0.218	0.1377	0.0044	0.61785	1675	42	831	25	667	20
161	DGR-3-9.3 bk lmst	13.11	35.84	0.01	105.240	1.650	1.3666	0.0171	0.79867	4737	16	5553	47	3194	214
162	DGR-3-9.4 br lmst	0.87	0.60	0.08	23.291	1.096	0.3438	0.0149	0.92428	3239	45	1905	71	918	70
163	DGR-3-1B.1	0.04	0.00	0.25	1.054	0.268	0.0245	0.0016	0.25998	731	125	156	10	104	17
164	DGR-3-1B.2	0.06	0.00	0.15	0.447	0.115	0.0171	0.0009	0.20420	375	78	110	6	90	7
165	DGR-3-1B.3	0.06	0.00	0.30	1.340	0.185	0.0212	0.0010	0.35840	863	78	135	7	65	12
166	DGR-3-2B.1	0.03	0.00	0.37	2.671	0.368	0.0381	0.0026	0.49175	1321	98	241	16	100	22
167	DGR-3-3B.1	0.03	0.00	0.14	-0.002	0.281	0.0130	0.0016	0.10000	-2	252	83	10	88	18
	DGR-6-886.91B Drill core														
168	DGR-6-3.2	0.13	0.02	1.03	0.900	0.110	0.0739	0.0021	0.23751	652	57	460	13	441	10
169	DGR-6-3.3	0.09	0.02	-19	1.682	0.215	0.0843	0.0031	0.29118	1002	78	522	19	464	15
170	DGR-6-3.4	0.06	0.01	0.95	6.029	0.566	0.0920	0.0052	0.60350	1980	80	567	31	264	33
171	DGR-6-3.4 br lmst	0.15	0.60	5.12	218.446	5.714	2.0121	0.0453	0.86024	5474	26	7108	97	682	326
172	DGR-5-2.3 bk lmst	0.91	0.89	2.53	49.015	2.568	0.4911	0.0246	0.95469	3972	51	2576	105	420	149
173	DGR-6-1.1	0.07	0.04	0.92	28.738	4.406	0.2866	0.0393	0.89393	3445	142	1625	194	239	260
174	DGR-6-1.2	0.29	1.05	1.94	202.281	11.618	1.8146	0.1007	0.96604	5396	57	6671	227	316	696

Table 3: ID-TIMS U-Pb Isotopic Data from Vein Calcite in Carbonate Collected from the Area of the Bruce Nuclear Site

No.	Sample	Wt. (mg)	U (ppm)	Pbtot (pg)	%Pb^{206} Com	^{238}U/^{204}Pb	^{206}Pb/^{204}Pb	2 Sig	^{207}Pb/^{204}Pb	2 Sig	Rho76	^{207}Pb/^{235}U Age (Ma)	2 Sig	^{206}Pb/^{238}U Age (Ma)	2 Sig	RhoC
	DGR-3-034-61															
1	dwd5771	8	0.074	38	47.2	1303.9	40.66	0.81	16.85	0.08	0.6673	124	61	109	4	0.01158
2	dwd5772	33	0.050	91	49.9	1468.9	37.68	0.28	16.65	0.04	0.5399	94	55	84	3	0.00401
	DGR-5-706-801															
3	dwd5774	2	0.040	70	80.9	77.6	23.28	0.10	15.84	0.05	0.6663	--	--	--	--	--
4	dwd5775	0.8	0.005	56	95.1	4.51	19.87	0.06	15.71	0.04	0.7058	--	--	--	--	--
	DGR-6-756-48B															
5	dwd5777	1.4	0.078	67	69.7	117.6	27.06	0.16	16.14	0.05	0.5565	480	527	451	38	0.00529
6	dwd5778	0.08	2.102	186	79.3	58.5	23.52	0.06	15.91	0.04	0.8040	--	--	--	--	--
	DGR-6-886-91B															
7	dwd5776	1.9	0.001	81	100.0	1.55	18.68	0.05	15.69	0.04	0.8444	--	--	--	--	--
	DD12-12FV															
8	dwd5911	3.1	0.1	31	59.0	1064	33.91	1.29	16.35	0.10	0.6973	92.2	77.0	92.5	4.5	0.0136
9	dwd5912	0.8	0.3	34	78.9	539	25.03	0.49	16.00	0.13	0.5533	--	--	--	--	--
10	dwd5913	1.0	1.3	43	50.9	2553	38.60	1.26	16.55	0.09	0.7436	49.9	33.0	50.5	1.9	0.0092
	DD12-11SE															
11	dwd5914	2.4	0.3	26	35.0	2740	59.42	5.28	17.62	0.29	0.9268	97.3	29.7	95.6	1.8	0.0337
12	dwd5916A	1.5	0.4	9	10.8	16736	253.5	142.5	26.60	6.71	0.9965	87.9	6.6	89.9	0.5	0.4132
13	dwd5916B	1.5	0.4	11	19.4	8856	142.81	80.82	21.32	3.73	0.9962	86.4	10.4	89.9	0.6	0.2311
14	dwd5917	0.7	0.6	21	53.1	1562	39.28	2.81	16.68	0.22	0.7455	90.9	53.3	85.1	3.1	0.0566

FOOTNOTES TO TABLE 3

Fraction label gives ppmU and age measured by LA-ICPMS on the corresponding grain

Pb-Pb and U-Pb ratios corrected for fractionation, blank and spike

U-Pb ages corrected for fractionation, blank, spike and initial common Pb

PbTot – common Pb assuming isotopic composition of laboratory blank: 206/204 – 18.221; 207/204 – 15.612; 208/204 – 39.360 (errors of 2%)

%Pb206 Com – percent of total 206Pb that is initial common Pb

Rho76 – error correlation coefficient for Pb 207/204 vs. 206/204 coordinates

RhoC – error correlation coefficient for Concordia coordinates

Concordia coordinates: Y = 206Pb/238U = EXP(L238*(206-238Age)) – 1; X = 207Pb/235U = EXP(L235*(207-235Age)) – 1

207Pb/206Pb = 137.88*X/Y; Uranium decay constants (L238 & L235) are from Jaffey et al. (1971)